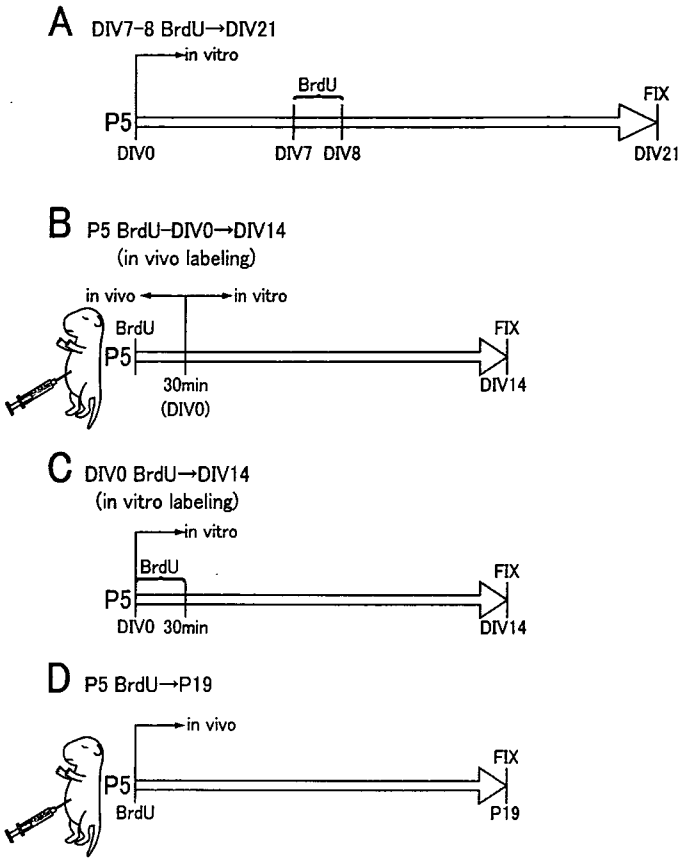

Fig. 1. Schematic drawing of time course of BrdU labeling. **A–C:** For slice culture experiments, newly generated cells were labeled by three methods: (A) incubation in culture medium containing 1 μM BrdU for 1 day after 7 days of in vitro culture (DIV), (B) an i.p injection of bromodeoxyuridine (BrdU) into P5 rats at the time point of 30 min before slice preparation, or (C) incubation in culture medium containing 1 μM BrdU for 30 min from the beginning of culture. Fourteen days after the BrdU treatment, the cultured slices were fixed. **D:** For the in vivo experiments, rats on postnatal day 5 (P5) were given an intraperitoneal injection of BrdU and fixed 14 days after the injection (P19).

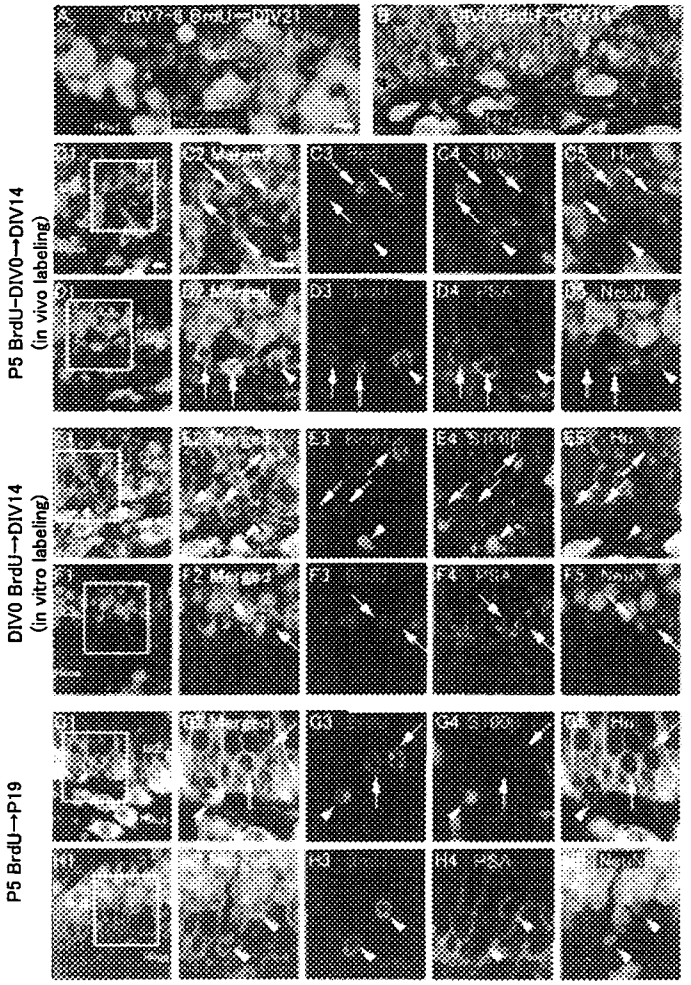

Fig. 2. Phenotypic analysis of BrdU-positive cells in a cultured slice that was treated with BrdU for 1 day after 7 days of in vitro culture (A), for 30 min before (in vivo BrdU treatment, C and D) or after (in vitro BrdU treatment, B, E, and F) the beginning of culture and fixed 14 days after treatment and of rats injected with BrdU on P5 and fixed 14 days (P19) after injection (G and H). **A, B:** Most BrdU-labeled cells were negative for neuronal marker Hu when newly generated cells were labeled during DIV7-8 (A). However, the newly generated cells labeled at the beginning of culture were positive for Hu (B). **C–F:** In the cultured slices, more than half the BrdU-positive cells in the GCL were positive for neuronal markers such as Hu (C and E, arrows), PSA-NCAM/NeuN (D and F, arrows), and NeuN (D, arrowheads). A small population of BrdU-positive cells in the GCL was positive for astrocytic marker S100β (C and E, arrowhead). **G, H:** Fourteen days after BrdU injection in vivo, about two-thirds of the BrdU-positive cells in the GCL were positive for neuronal markers such as Hu (G, arrows) and NeuN (H, arrowheads). Scale bar = 10 μm applies to B in A, to D1–H1 in C1, and to D2–H2 in C2.

positive oligodendrocytes and BrdU/Ki67-double-positive proliferating cells were very low (data not shown). As it has been reported that in in vivo conditions about two-thirds of precursor cells differentiate into neurons in the early postnatal period (Namba et al., 2005) and in the adult hippocampus (Kempermann et al., 2003), the results indicate that neuronal production is very low in proliferative neural precursor cells after 7 days in culture.

In Vivo– and Early In Vitro–Labeled Cultures. To search for suitable labeling methods of neural precursor cells that lead to efficient neuronal production, we attempted to use two different methods: in vivo–labeled (Fig. 1B) and early in vitro–labeled (Fig. 1C) cultures. Further, to precisely ascertain the efficiency of neuronal production, we compared the results of these two cultures with those of living age-matched rats.

To determine whether the in vitro condition itself affects the capacity for neuronal differentiation, in the first in vivo–labeled cultures, proliferative neural precursor cells were labeled in vivo, and then hippocampal slices were cultured to allow the in vivo–labeled precursors

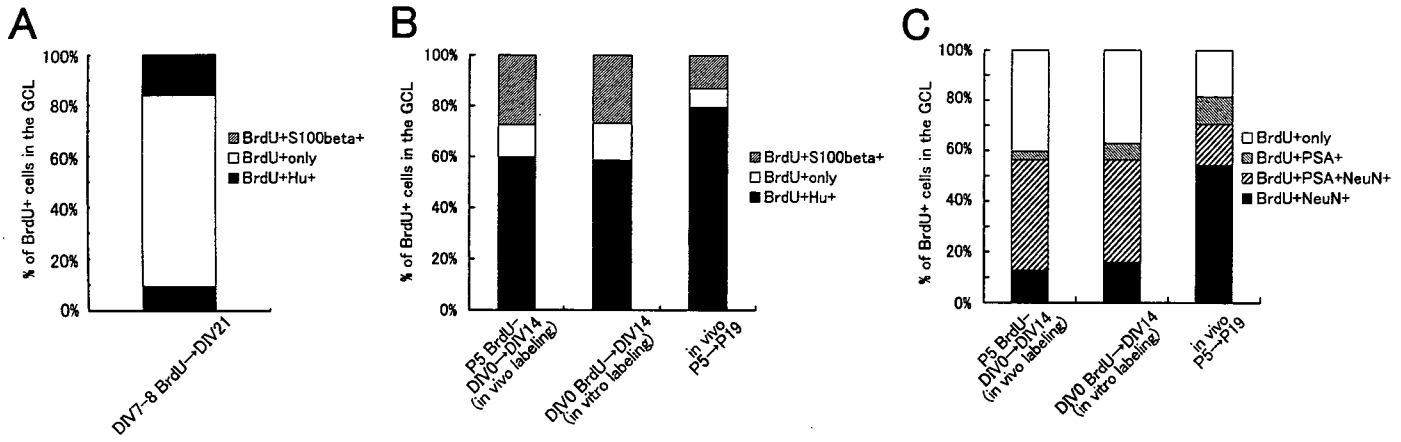

Fig. 3. Quantitative analysis of neurogenesis in cultured slices and in vivo. **A:** In the late in vitro–labeled culture, newly generated cells were labeled by BrdU during DIV7-8. Only about 10% of these BrdU-labeled cells were positive for the neuronal marker Hu. **B, C:** Comparison of neurogenic ability in the cultured slices and in vivo. Cultured slices were treated with BrdU before (in vivo labeled, Fig. 1B) or after (in vitro labeled, Fig. 1C) initiation of the culture. For the in vivo experiments, P5 rats were injected with BrdU and fixed 14 days after the injection (Fig. 1D). **B:** In the cultured slices, about 60% of the BrdU-positive cells in the GCL expressed Hu and about 30% of the BrdU-labeled cells were positive for S100β. **C:** To clarify the degree of neuronal maturation, the percentage of BrdU-labeled cells that coexpressed immature (PSA-NCAM) and/or mature (NeuN) neuronal markers in the granule cell layer and hilus was quantified. The percentage of mature neurons (NeuN+/BrdU+) in the cultured slices was lower than that in vivo. However, the percentage of immature neurons (PSA+/NeuN+/BrdU+ and PSA+/NeuN-/BrdU+) was higher than that in vivo.

to differentiate into neurons in vitro. P5 rats were injected with BrdU 30 min before slice preparation (Fig. 1B), and hippocampal slices were cultured for 14 days. At the end of the culture period, most BrdU-labeled cells were in the GCL (56.9% ± 3.3%, n = 21 slices from 3 rats; Fig. 4). More than half the BrdU-labeled cells in the GCL expressed immature and mature neuronal marker Hu (60.1% ± 3.7%), and the other cells were S100β positive (27.7% ± 3.0%) and double negative (12.8% ± 2.3%, n = 21 slices from 3 rats; Figs. 2C, 3B). In the living age-matched rats injected with BrdU on P5 and fixed on P19, most of these BrdU-labeled newly generated cells were in the GCL on P19 (Fig. 4). The BrdU-labeled cells in the GCL were mainly positive for Hu (79.1% ± 0.8%), with a small proportion positive for S100β (13.0% ± 1.5%) or double negative (7.4% ± 1.1%, n = 5 rats; Figs. 2G, 3B). Although the proportion of Hu-positive neuronal cells in the early in vitro–slice culture was smaller by 19% than that in age-matched rats ($P < 0.05$), the proportion was 7-fold higher than that in the late in vitro culture ($P < 0.001$). These results suggest that neural precursor cells labeled in vivo can differentiate into neurons more efficiently in cultured slices than in a late in vitro–labeled culture and that the in vitro condition itself is not the cause of the low rate of neuronal differentiation.

To determine whether precursor cells labeled early in the culture can differentiate into neurons, the hippocampal slices were labeled in vitro with BrdU for 30 min at the beginning of the culture and were cultured for 14 days to allow the in vitro–labeled precursors to differentiate into neurons in vitro. Similar to the results in the in vivo–labeled cultures, most BrdU-labeled cells were in the GCL after 14 divisions (62.6% ± 3.8%, n = 10 slices from 4 rats; Fig. 4). More than two-thirds of the BrdU-labeled cells in the GCL expressed immature and mature neuronal marker Hu (58.5% ± 3.1%), and the others were S100β positve (26.5% ± 2.4%) and double negative (12.8% ± 2.3%, = 10 slices from 4 rats; Figs. 2B,E, 3B). These results suggest that neural precursors labeled early in cultures can differentiate into neurons efficiently.

Further, the neuronal maturation of the BrdU-labeled cells was assessed by a mature neuronal marker, NeuN, and an immature neuronal marker, PSA-NCAM (Seki and Arai, 1993; Seki, 2002). In the in vivo–labeled cultures, most of the BrdU-labeled cells in the GCL were positive for both PSA-NCAM and NeuN (43.7% ± 3.2%, n = 10 slices from 3 rats), and a minority of the cells were positive only for PSA-NCAM (3.2% ± 1.1%) or for NeuN (12.7% ± 3.6%; n = 10 slices from 3 rats; Figs. 2D, 3C). Similarly, in the early in vitro–labeled cultures, most of the BrdU-labeled cells were positive for both PSA-NCAM and NeuN (40.5% ± 3.7%), and a minority of the cells were positive only for PSA-NCAM (6.6% ± 1.5%) or for NeuN (15.7% ± 3.9%, n = 10 slices from 3 rats; Figs. 2F, 3C). There was almost no difference in the efficiency of neuronal production between the two labeling methods performed just before or soon after initiation of the cultures. However, the proportion of NeuN-positive mature neurons in these two cultures was significantly smaller than that in the living age-matched rats (54.5% ± 7.1%) that were labeled with BrdU on P5 and fixed on P19. Conversely, the proportion of immature neurons in these two cultures was higher than that in the

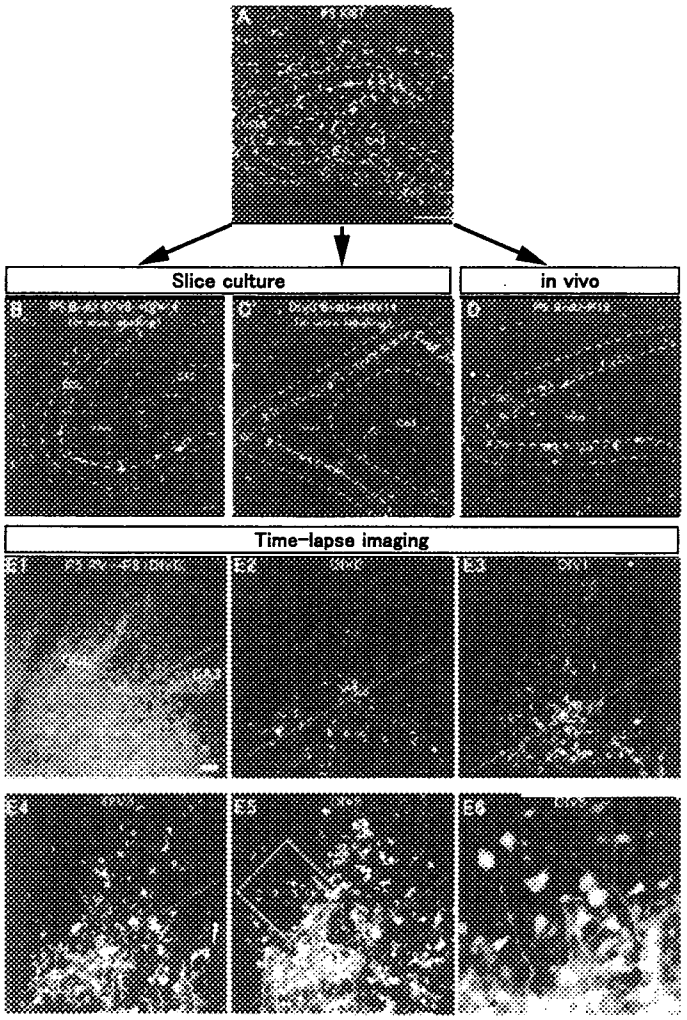

Fig. 4. Distribution of Ki67-positive (P5) cells (A) and BrdU-labeled cells in rats injected with BrdU on P5 and fixed 14 days (P19, D) days after injection and in the cultured slices treated with BrdU for 30 min before (in vivo BrdU treatment, B) or after (in vitro BrdU treatment, C) the beginning of culture and fixed 14 days after treatment. Dotted lines indicate GCL and the CA3 field of the pyramidal cell layer. **A:** Ki67-positive proliferating cells were found throughout the entire dentate gyrus on P5. **B–D:** Most of the newly generated (BrdU-labeled) cells were in the GCL, suggesting that the newly generated cells migrated toward the GCL in the cultured slices (B, C) and in vivo (D). **E:** Time-lapse imaging showing migration of hilar precursor cells to the GCL. Retrovirus vector–bearing *EGFP* gene was directly injected into the hilus. The red lines passing through the hippocampal crest and the CA3 pyramidal cell layer indicate the border of the suprapyramidal and infrapyramidal regions. Scale bar = 100 μm in A applies to B, C, and D; 50 μm in E1.

age-matched rats (16.5% ± 2.2% BrdU+/PSA+/NeuN+ cells and 10.9% ± 3.7% BrdU+/PSA+ cells, n = 3 rats; Figs. 2H, 3C). These results suggest that neural precursor cells labeled early in culture can differentiate into neurons efficiently under culture conditions, although maturation of differentiated neurons was somewhat delayed in the two cultures.

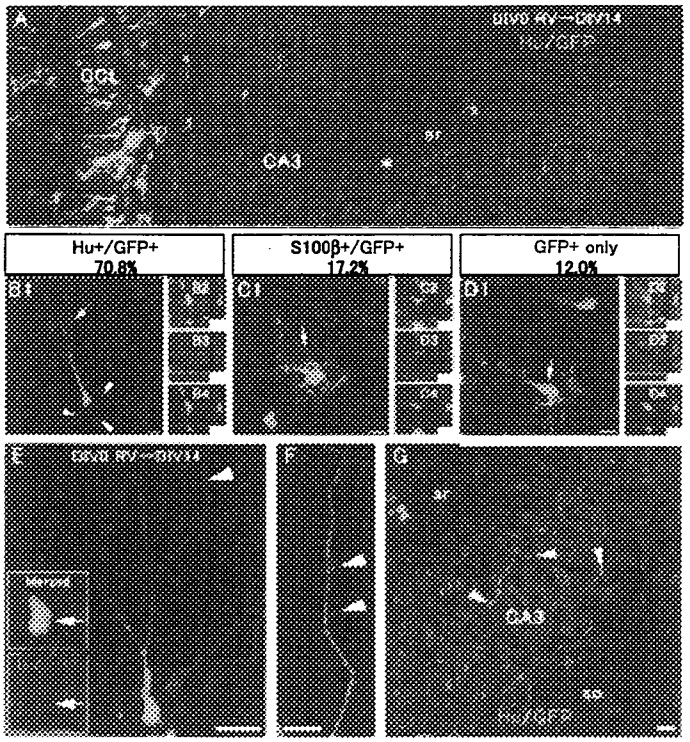

Fig. 5. Phenotypic and morphological analysis of RV-positive cells (GFP-positive cells) in cultured slices treated with RV at the beginning of the culture and fixed 14 days after treatment. **A:** Most GFP+ cells were in the GCL and extended axons (mossy fibers), indicated by an asterisk. **B:** Most GFP-positive cells in the GCL (70.8%) expressed Hu, a neuronal marker. These cells extended apical dendrites (arrow) and some basal dendrites or axons (arrowhead), suggesting that these Hu-/GFP-positive cells possessed the features of typical immature granule cells. **C:** About one-fifth of the GFP-positive cells were positive for the astrocytic marker S100β (arrow). These possessed highly branched processes. **D:** A small population of the GFP-positive cells in the GCL was negative for both Hu and S100β. The density of the branched processes of GFP-single-positive cells was lower than that of the S100β-/GFP-positive cells. **E:** GFP-positive cell in the GCL expressed Hu (arrows in inset) and extended apical dendrites. **F:** Apical dendrite (arrowhead in E) showing a few spines (arrowheads). **G:** GFP-positive axons (mossy fibers) found in the CA3 region of the PCL, with arrowheads showing some boutons (sr, stratum radiatum; so, stratum oriens). B2, C2, and D2 are merged images of B3-4, C3-4, and D3-4, respectively. Scale bar = 20 μm for E and G;10 μm for B1, C1, D1, and F; and 5 μm for B2-4, C2-4, and D2-4.

Retrovirus-EGFP Labeling

To examine whether newly generated cells develop into normal-shaped granule cells, we labeled dividing cells with our modified high-titer retroviral vector (RV) carrying enhanced green fluorescent protein (GFP; Namba et al., 2005). Because the BrdU-labeling experiments showed that early in vitro labeling induced efficient neuronal differentiation of precursor cells, retrovirus labeling was performed at the beginning of the slice cultures.

Similar to the results with BrdU-labeled cells, most retroviral-labeled cells (GFP-positive cells) were in GCL (75.1%, n = 489 cells; Fig. 5A) after14 divisions, and these cells expressed Hu (70.8%, n = 367 cells; Fig. 5B). Other GFP-labeled cells in the GCL were positive for S100β (17.2%) or not positive for either marker (12.0%; Fig. 5C,D). The retrovirus labeling clearly demonstrated that GFP-/Hu-positive neuronal cells extended dendrites with a few spines (Fig. 5B,E,F) and also gave rise to axons with boutons toward the CA3 region of the pyramidal cell layer (Fig. 5A,G). To assess the in vitro maturation of the newly generated GFP-/Hu-double-positive cells in detail, the length and branching points of the dendrites were examined and compared with those that matured in vivo in living rats. In the GFP-labeled granule cells that matured in vitro, mean total dendrite length was 301.6 ± 15.7 μm, and mean number of branching points was 5.45 ± 0.31 (n = 11 cells). These values were higher in GFP-labeled granule cells that matured in living animals that were labeled with retrovirus-GFP on P5 and fixed on P19 (mean length 614.3 ± 14.8 μm, mean number of branching points 7.36 ± 0.20, n = 11 cells). These results suggest that new cells generated in slice cultures develop into normal dentate granule cells, but their maturation can be somewhat delayed compared with in vivo maturation.

Time-Lapse Imaging

One advantage of slice culture experiments is being able to observe the migration of labeled cells using the same slices. In the present study, we tried to examine whether the migration of neural precursors suggested by the BrdU experiments (Fig. 4) could be observed in the present culture system. Retrovirus-EGFP was injected into the hilus of P5 rats. Hippocampal slices (n = 14 slices from 10 rats) were cultured 3 days after the retroviral injection on P5 and were observed every day. A small population of EGFP-labeled cells was distributed in the hilus at DIV 0 (Fig. 4E1), and thereafter, the labeled cells increased in number from DIV 1 to DIV 5. Simultaneously, a distinct population of labeled cells appeared in the subgranular zone and granule cell layer, and the numbers of these labeled cells increased (Fig. 4E2–5). Finally, the labeled cells developed apical dendrites at DIV 5 (Fig. 4E6). The time-lapse imaging directly demonstrated that the neural precursors migrated from the hilus to the granule cell layer.

DISCUSSION

In research on postnatal neurogenesis using organotypic hippocampal slice cultures, it is important to know the extent to which cultured slices possess neurogenic capacity. In the present study, we have shown that at the beginning of the cultures, neural precursor cells had a high neurogenic capacity that was similar to that of age-matched rats. However, after 7 days in culture, the neural precursor cells lost their high neurogenic capacity, although they still exhibited a low rate of neuronal production. This indicates that although cultured hippocampal slices are generally used in electrophysiological and pharmacological studies after 1–2 weeks in culture (Okada et al., 1995), the late in vitro labeling of proliferative precursors has the disadvantage of requiring a high rate of proliferating activity of neural precursors for analysis. On the other hand, because in vivo and early in vitro labeling of proliferative neural precursors allows efficient neuronal differentiation of labeled precursors, these types of labels are suitable methods for studies that need a greater chance to observe neuronal production in organotypic hippocampal slice cultures.

Late In Vitro–Labeled Culture

The findings of the present experiments indicate that in late in vitro labeling, only a small number of proliferative neuronal precursors differentiated into neurons, with most becoming nonneuronal cells. In this regard, previous reports have shown that nonneuronal cells such as astrocytes, microglia, and fibroblasts continue to proliferate in organotypic hippocampal slice cultures (del Rio et al., 1991; Gahwiler et al., 1997; Raineteau et al., 2004). This suggests that the cellular composition of cells proliferating in cultured hippocampal slices is considerably different than that in vivo. Proliferative activity is also reported to be reduced over the first 7 days in culture (Hajos et al., 1994; Sadgrove et al., 2006). Furthermore, published studies have reported conflicting results about the capacity for neuronal production after 1–2 weeks in organotypic hippocampal slice cultures. Raineteau et al. (2004) showed that despite more than 80% of proliferating cells labeled with BrdU being GFAP positive at 14 DIV, a small proportion of proliferating cells still could differentiate into neurons and that the rate of the neuronal differentiation was enhanced by EGF and the serum-free conditions. Similarly, Kamada et al. (2004) indicated that among proliferative cells labeled with retrovirus-EGFP at 14 DIV, a quarter of the EGFP- positive cells expressed NeuN and Tuj1 2 weeks after infection. Poulsen et al. (2005) reported that dividing cells labeled with BrdU at 12–16 DIV did not give rise to TUC-4-positive neuronal cells. Laskowski et al. (2005) revealed that bFGF and EGF stimulated proliferation of cells labeled at 7–9 DIV, but not neurogenesis. Taken together, these findings suggest that although neuronal production occurs under certain culture conditions in late in vitro–labeled cultures, the rate of neuronal production is relatively low. Late in vitro–labeled cultures could be useful for examining a small number of newly generated cells differentiate into neurons.

In Vivo– and Early In Vitro–Labeled Cultures

Our previous report showed that P5 proliferative precursor cells are mainly in the hilus and express astrocytic markers (Namba et al., 2005). During their developmental period, they migrate to the granule cell layer and become granule neurons. In the in vivo and early in vitro-labeled slice culture experiments, most of the

proliferating cells that had been labeled in vivo on P5 or early in vitro were found in the granule cell layer at 14 DIV, and neuronal production was much more efficient than that in the late in vitro–labeled cultures. Furthermore, retrovirus-EGFP labeling and time-lapse imaging indicated that the hilar neural precursor cells migrated to the granule cell layer and finally differentiated into normal granule cells. Therefore, the in vivo–like capacity of neural precursor cells for neuronal production could persist in hippocampal slices early in the culture period, and then during the culture period, the capacity for migration and differentiation could also be maintained under culture conditions. On the other hand, during the culture period, the capacity of neural precursors for neuronal production would be reduced. Note also that in experiments using embryonic neocortical slices, cell proliferation, differentiation, and migration generally are examined during the early culture period (Miyata et al., 2001; Noctor et al., 2001). Collectively, these results show that in vivo– and early in vitro–labeled cultures are useful for studying the developmental dynamics of the hippocampus.

Application and Limits of Hippocampal Slice Culture for Postnatal and Adult Neurogenesis Model

As in hippocampal slice cultures, hippocampal slices are taken from early postnatal rats, the development of newly generated cells in slice cultures represents postnatal neurogenesis. However, the results of the hippocampal slice cultures could provide some information on the developmental mechanism of adult neurogenesis because early postnatal and adult neurogenesis have some similarities. In the adult, it has been demonstrated that proliferation of neural precursors occurs in the subgranular zone (Altman and Das, 1965; Seki, 2002), and the precursor cells expressing GFAP give rise to neurons (Seri et al., 2001). Similarly, in the postnatal hippocampus, proliferating precursors are found in the subgranular zone, although they are predominantly in the hilus (Altman and Bayer, 1990; Namba et al., 2005), and precursor cells positive for astrocytic markers produce neurons (Namba et al., 2005). Thus, it is probable that adult-like neuronal differentiation from astrocytic precursors can be examined in the hilus and the subgranular zone of the postnatal hippocampus, and that adult-like neuronal migration and neurite formation can be observed in the subgranular zone. Further studies are needed to define the extent to which neurogenesis in hippocampal organotypic slice cultures represents adult neurogenesis.

In addition, new cells raised in vitro exhibited delayed neuronal maturation. The underlying reason for this delay remains obscure. Maturation of newly generated neurons may require some growth factors or input from extrahippocampal regions such as the entorhinal cortex and septum. However, retrovirus labeling indicated that the newly generated neurons extended axons with large boutons, exhibiting the typical features of mossy fibers and dendrites with spines. This suggests functional incorporation of newly generated neurons into the hippocampal network. In this respect, Raineteau et al. (2006) demonstrated electrophysiologically that new granule cells arising in organotypic hippocampal slice cultures mature and integrate normally into the hippocampal circuitry (Raineteau et al., 2006). Therefore, the early in vitro–labeled cultures used in the present study could provide a useful ex vivo model in the search for the mechanism of granule cell maturation.

ACKNOWLEDGMENTS

We thank Drs. Hirotaka J. Okano (Keio University) and Robert B. Darnell (The Rockefeller University) for anti-Hu antibody, Nobuaki Tamamaki (Kumamoto Univeristy) for the anti-GFP antibody and Harumi Kaneko (Keio University) for nice illustrations. The authors appreciate the review of the manuscript prior to submission by Dr. Alison Murray. This study was supported by Grant-in-Aid for Scientific Research 17500238 from the Japan Society for the Promotion of Science and in part by a High Technology Research Center Grant from the Japanese Ministry of Education, Culture, Sports and Science.

REFERENCES

Altman J, Bayer SA. 1990. Migration and distribution of two populations of hippocampal granule cell precursors during the perinatal and postnatal periods. J Comp Neurol 301:365–381.

Altman J, Das GD. 1965. Autoradiographic and histological evidence of postnatal hippocampal neurogenesis in rats. J Comp Neurol 124:319–335.

del Rio JA, Heimrich B, Soriano E, Schwegler H, Frotscher M. 1991. Proliferation and differentiation of glial fibrillary acidic protein-immunoreactive glial cells in organotypic slice cultures of rat hippocampus. Neuroscience 43:335–347.

Eriksson PS, Perfilieva E, Bjork-Eriksson T, Alborn AM, Nordborg C, Peterson DA, Gage FH. 1998. Neurogenesis in the adult human hippocampus. Nat Med 4:1313–1317.

Gahwiler BH, Capogna M, Debanne D, McKinney RA, Thompson SM. 1997. Organotypic slice cultures: a technique has come of age. Trends Neurosci 20:471–477.

Gould E, Beylin A, Tanapat P, Reeves A, Shors TJ. 1999. Learning enhances adult neurogenesis in the hippocampal formation. Nat Neurosci 2(3):260–265.

Gould E, McEwen BS, Tanapat P, Galea LA, Fuchs E. 1997. Neurogenesis in the dentate gyrus of the adult tree shrew is regulated by psychosocial stress and NMDA receptor activation. J Neurosci 17:2492–2498.

Hajos F, Balazs R, Baker RE, Gerics B, Nuijtinck R. 1994. Structural maturation, cell proliferation and bioelectric activity in long-term slice-cultures of immature rat hippocampus. Int J Dev Neurosci 12:87–97.

Kamada M, Li RY, Hashimoto M, Kakuda M, Okada H, Koyanagi Y, Ishizuka T, Yawo H. 2004. Intrinsic and spontaneous neurogenesis in the postnatal slice culture of rat hippocampus. Eur J Neurosci 20:2499–2508.

Kempermann G, Gast D, Kronenberg G, Yamaguchi M, Gage FH. 2003. Early determination and long-term persistence of adult-generated new neurons in the hippocampus of mice. Development 130:391–399.

Kuhn HG, Dickinson-Anson H, Gage FH. 1996. Neurogenesis in the dentate gyrus of the adult rat: age-related decrease of neuronal progenitor proliferation. J Neurosci 16:2027–2033.

Laskowski A, Schmidt W, Dinkel K, Martinez-Sanchez M, Reymann KG. 2005. bFGF and EGF modulate trauma-induced proliferation and neurogenesis in juvenile organotypic hippocampal slice cultures. Brain Res 1037(1–2):78–89.

Liu J, Solway K, Messing RO, Sharp FR. 1998. Increased neurogenesis in the dentate gyrus after transient global ischemia in gerbils. J Neurosci 18:7768–7778.

Malberg JE, Eisch AJ, Nestler EJ, Duman RS. 2000. Chronic antidepressant treatment increases neurogenesis in adult rat hippocampus. J Neurosci 20:9104–9110.

Miyata T, Kawaguchi A, Okano H, Ogawa M. 2001. Asymmetric inheritance of radial glial fibers by cortical neurons. Neuron 31:727–741.

Namba T, Mochizuki H, Onodera M, Mizuno Y, Namiki H, Seki T. 2005. The fate of neural progenitor cells expressing astrocytic and radial glial markers in the postnatal rat dentate gyrus. Eur J Neurosci 22:1928–1941.

Noctor SC, Flint AC, Weissman TA, Dammerman RS, Kriegstein AR. 2001. Neurons derived from radial glial cells establish radial units in neocortex. Nature 409:714–720.

Okada M, Sakaguchi T, Kawasaki K. 1995. Correlation between anti-ubiquitin immunoreactivity and region-specific neuronal death in N-methyl-D-aspartate-treated rat hippocampal organotypic cultures. Neurosci Res 22:359–366.

Okano HJ, Darnell RB. 1997. A hierarchy of Hu RNA binding proteins in developing and adult neurons. J Neurosci 17:3024–3037.

Palmer TD, Takahashi J, Gage FH. 1997. The adult rat hippocampus contains primordial neural stem cells. Mol Cell Neurosci 8:389–404.

Palmer TD, Willhoite AR, Gage FH. 2000. Vascular niche for adult hippocampal neurogenesis. J Comp Neurol 425:479–494.

Parent JM, Yu TW, Leibowitz RT, Geschwind DH, Sloviter RS, Lowenstein DH. 1997. Dentate granule cell neurogenesis is increased by seizures and contributes to aberrant network reorganization in the adult rat hippocampus. J Neurosci 17:3727–3738.

Poulsen FR, Blaabjerg M, Montero M, Zimmer J. 2005. Glutamate receptor antagonists and growth factors modulate dentate granule cell neurogenesis in organotypic, rat hippocampal slice cultures. Brain Res 1051(1–2):35–49.

Raineteau O, Hugel S, Ozen I, Rietschin L, Sigrist M, Arber S, Gahwiler BH. 2006. Conditional labeling of newborn granule cells to visualize their integration into established circuits in hippocampal slice cultures. Mol Cell Neurosci 32:344–355.

Raineteau O, Rietschin L, Gradwohl G, Guillemot F, Gahwiler BH. 2004. Neurogenesis in hippocampal slice cultures. Mol Cell Neurosci 26:241–250.

Sadgrove MP, Laskowski A, Gray WP. 2006. Examination of granule layer cell count, cell density, and single-pulse BrdU incorporation in rat organotypic hippocampal slice cultures with respect to culture medium, septotemporal position, and time in vitro. J Comp Neurol 497:397–415.

Sakaguchi T, Okada M, Kuno M, Kawasaki K. 1997. Dual mode of N-methyl-D-aspartate-induced neuronal death in hippocampal slice cultures in relation to N-methyl-D-aspartate receptor properties. Neuroscience 76:411–423.

Schmidt-Hieber C, Jonas P, Bischofberger J. 2004. Enhanced synaptic plasticity in newly generated granule cells of the adult hippocampus. Nature 429:184–187.

Seaberg RM, van der Kooy D. 2002. Adult rodent neurogenic regions: the ventricular subependyma contains neural stem cells, but the dentate gyrus contains restricted progenitors. J Neurosci 22:1784–1793.

Seki T. 2002. Hippocampal adult neurogenesis occurs in a microenvironment provided by PSA-NCAM-expressing immature neurons. J Neurosci Res 69:772–783.

Seki T. 2003. Microenvironmental elements supporting adult hippocampal neurogenesis. Anat Sci Int 78:69–78.

Seki T, Arai Y. 1991. Expression of highly polysialylated NCAM in the neocortex and piriform cortex of the developing and the adult rat. Anat Embryol (Berl) 184:395–401.

Seki T, Arai Y. 1993. Highly polysialylated neural cell adhesion molecule (NCAM-H) is expressed by newly generated granule cells in the dentate gyrus of the adult rat. J Neurosci 13:2351–2358.

Seki T, Arai Y. 1995. Age-related production of new granule cells in the adult dentate gyrus. Neuroreport 6:2479–2482.

Seri B, Garcia-Verdugo JM, McEwen BS, Alvarez-Buylla A. 2001. Astrocytes give rise to new neurons in the adult mammalian hippocampus. J Neurosci 21:7153–7160.

Stoppini L, Buchs PA, Muller D. 1991. A simple method for organotypic cultures of nervous tissue. J Neurosci Methods 37(2):173–182.

Suzuki A, Obi K, Urabe T, Hayakawa H, Yamada M, Kaneko S, Onodera M, Mizuno Y, Mochizuki H. 2002. Feasibility of ex vivo gene therapy for neurological disorders using the new retroviral vector GCDNsap packaged in the vesicular stomatitis virus G protein. J Neurochem 82:953–960.

Tamamaki N, Nakamura K, Furuta T, Asamoto K, Kaneko T. 2000. Neurons in Golgi-stain-like images revealed by GFP-adenovirus infection in vivo. Neurosci Res 38(3):231–236.

Tanaka R, Yamashiro K, Mochizuki H, Cho N, Onodera M, Mizuno Y, Urabe T. 2004. Neurogenesis after transient global ischemia in the adult hippocampus visualized by improved retroviral vector. Stroke 35:1454–1459.

Tashiro A, Sandler VM, Toni N, Zhao C, Gage FH. 2006. NMDA-receptor-mediated, cell-specific integration of new neurons in adult dentate gyrus. Nature 442:929–933.

Tozuka Y, Fukuda S, Namba T, Seki T, Hisatsune T. 2005. GABAergic excitation promotes neuronal differentiation in adult hippocampal progenitor cells. Neuron 47:803–815.

van Praag H, Schinder AF, Christie BR, Toni N, Palmer TD, Gage FH. 2002. Functional neurogenesis in the adult hippocampus. Nature 415:1030–1034.

International Immunology, Vol. 19, No. 5, pp. 609–619
doi:10.1093/intimm/dxm026

© The Japanese Society for Immunology. 2007. All rights reserved.
For permissions, please e-mail: journals.permissions@oxfordjournals.org

An RNA-binding protein αCP-1 is involved in the STAT3-mediated suppression of NF-κB transcriptional activity

Hitomi Nishinakamura[1], Yasumasa Minoda[1], Kazuko Saeki[1], Keiko Koga[1], Giichi Takaesu[1], Masafumi Onodera[2], Akihiko Yoshimura[1] and **Takashi Kobayashi[1]**

[1]Division of Molecular and Cellular Immunology, Medical Institute of Bioregulation, Kyushu University, 3-1-1 Maidashi, Higashi-ku, Fukuoka 812-8582, Japan
[2]Department of Hematology, Institute of Clinical Medicine, University of Tsukuba, Tsukuba 305-8575, Japan

Keywords: gene regulation, IL-10, lipopolysaccharide, NF-κB, signal transduction, STAT3, Toll-like receptor 4

Abstract

Signal transducer and activator of transcription 3 (STAT3) has been shown to mediate the anti-inflammatory effect of IL-10. Activated STAT3 suppresses LPS-induced IL-6, tumor necrosis factor-α and IL-12 gene expression in macrophages and dendritic cells. However, the mechanism of Toll-like receptor (TLR) signal suppression by STAT3 has not been clarified. In this study, we investigated the effect of constitutively activated STAT3 (STAT3C) on LPS-induced nuclear factor-κB (NF-κB) activation. The forced expression of STAT3C in HEK293/TLR4 cells, but neither wild-type STAT3 nor dominant-negative form of STAT3, suppressed LPS–TLR4-mediated NF-κB reporter activation. The over-expression of STAT3C did not affect the signal transduction of TLR4, such as the phosphorylation of inhibitory nuclear factor-κBα and mitogen-activated protein kinases and the DNA-binding activity of NF-κB. Thus, STAT3C could suppress the transcriptional and/or translational activity of NF-κB. To define the molecular mechanism, we searched STAT3C-binding proteins by using a proteomic approach and found that a novel RNA-binding protein, αCP-1, interacted with STAT3C. αCP-1 is a K-homology domain-containing RNA-binding protein with specificity for C-rich pyrimidine tracts. Such proteins play pivotal roles in a broad-spectrum of transcriptional and translational events. The over-expression of αCP-1 augmented the suppressive effect of STAT3C on NF-κB activation in HEK293/TLR4 cells. Furthermore, the forced expression of αCP-1 enhanced the antagonistic effect of IL-10 on IL-6 production in RAW264.7 cells, while small interfering RNA against αCP-1 reduced it. These data suggest that αCP-1 is involved in the STAT3-mediated suppression of NF-κB activity.

Introduction

IL-10 is a potent immunoregulatory cytokine with numerous effects on antigen-presenting cells (APCs), such as the down-regulation of pro-inflammatory cytokines, chemokines and co-stimulatory molecules. However, the mechanisms by which IL-10 exerts these effects remain largely unknown. Several mechanisms have been proposed for the IL-10-mediated inhibition of LPS-induced pro-inflammatory gene expression (1), including the activation of the heme oxygenase-1 carbon monoxide pathway (2) and the nuclear factor-κB (NF-κB) pathway (3), the inhibition of Akt activity (4) and the induction of B cell lymphoma-3 (Bcl-3) (5). However, the precise mechanisms remain controversial; specifically, the ability of IL-10 to inhibit LPS-induced gene expression has been shown to be transcriptionally mediated via the inhibition of the NF-κB pathway or a post-transcriptional mechanism via destabilizing mRNA. In the case of tumor necrosis factor-α (TNF-α), the latter effect requires the AU-rich elements in the 3′-untranslated region (6) and the *de novo* protein production responsible for mediating the stabilization of mRNA. IL-10 mediates its inhibitory effects by binding to its receptor complex, which induces the activation of the cytoplasmic receptor-associated tyrosine

Correspondence to: T. Kobayashi; E-mail: takashik@bioreg.kyushu-u.ac.jp

Transmitting editor: T. Watanabe

Received 4 January 2007, *accepted* 15 February 2007
Advance Access publication 22 March 2007

kinases, JAK1 and Tyk2 (1), followed by signal transducer and activator of transcription 3 (STAT3) phosphorylation, homodimerization and translocation to the nucleus, where it binds to STAT-binding elements in the promoters of various IL-10-inducible genes. The essential role of STAT3 in the effect of IL-10 has been clearly demonstrated by studies using a mouse model with the genetically deleted STAT3 gene in macrophages (7). The over-expression of a dominant-negative form of STAT3 (dnSTAT3) completely reversed the ability of IL-10 to inhibit LPS-mediated TNF-α and IL-6 production (8).

The obligate role of STAT3 in IL-10 signaling raises the vexing issue of pathway redundancy and specificity as many receptors utilize STAT3. For example, IL-6 signaling also activates the JAK1–STAT3 pathway, which is incapable of activating the anti-inflammatory response. Previously, we demonstrated that the suppressor of cytokine signaling 3 (SOCS3) causes the differences between IL-10 and IL-6 (9). SOCS3 is required to regulate STAT3 signaling from receptors such as gp130 (e.g. the IL-6 receptor), the leptin receptor and the G-CSF-R. In macrophages stimulated with either IL-6 or IL-10, SOCS3 expression is strongly induced. However, the inhibitory effects of SOCS3 are restricted to the gp130 subunit of the IL-6R, SOCS3 binds to phosphorylated Tyr757 of gp130 and thereby blocks signaling. In contrast, IL-10R appears refractory to the effects of SOCS3 because the SOCS3 SH2 domain does not bind to the IL-10R subunits (9). The results of our study suggest that the prolonged activation of STAT3 is necessary for the suppression of Toll-like receptor (TLR) signaling, while the transient activation of STAT3 is not sufficient for the suppression of TLR signaling. A similar result was recently obtained by using mutant STAT3-activating receptors lacking SOCS3-binding sites (10). This idea is also supported by the fact that constitutively activated STAT3 in many tumor cells suppresses pro-inflammatory cytokine and chemokine synthesis by suppressing NF-κB activity (11). *Toxoplasma gondii* activates STAT3 rapidly and independently of secreted factors that activate STAT3, such as IL-10 itself (12). The activation of STAT3 suppresses the ability of macrophages to produce the pro-inflammatory cytokines necessary to kill and control the parasite and presumably forms one element in *T. gondii*'s repertoire of survival tools. This information raises the possibility that prolonged, constitutively activated STAT3 is sufficient for the suppression of TLR signals. However, there is no direct evidence that activated STAT3 is sufficient for the suppression of LPS-induced gene regulation.

Thus, we examined the effect of STAT3C, a mutant form of constitutively activated STAT3, on TLR signaling and NF-κB activity. We found that STAT3C inhibits NF-κB transcriptional activity without affecting signaling pathways such as inhibitory nuclear factor-κBα (IκBα) phosphorylation and mitogen-activated protein kinases (MAPKs) activation. We sought STAT3C-binding proteins by a proteomic approach and identified several proteins, including an RNA-binding protein, αCP-1, which could augment the suppressive effect of STAT3C and IL-10. Our data suggest a novel mechanism for the transcriptional repressor activity of STAT3 for NF-κB activation and give rise to a novel approach to the suppression of inflammation.

Methods

Cells, antibodies and reagents

HEK293 cells stably expressing human *TLR4*, *MD2* and *CD14* genes (HEK293/TLR4) were purchased from Invivogen (San Diego, CA, USA). Bone marrow-derived dendritic cells (BMDCs) were prepared from mouse bone marrow cells as described (13). Culture supernatants containing recombinant mouse IL-10 were prepared from HEK293T cells transfected with mouse IL-10 cDNA in pME18S. The amount of IL-10 was determined by ELISA, and the activity of IL-10 was confirmed as the suppression of surface molecules on LPS-treated RAW264.7 or BMDC by FACS (data not shown). The anti-extracellular signal-regulated kinase (ERK)-2 (C-14), anti-Myc (9E10) antibodies and anti-αCP-1 goat polyclonal antibody (T-18) were purchased from Santa Cruz Biotechnology (Santa Cruz, CA, USA). The anti-phospho-ERK1/2 (9106), anti-FLAG (M2), anti-phospho-c-Jun N-terminal kinase (JNK) (9255), anti-phospho-p38 (9216), anti-JNK (9252), anti-p38 (9212), anti-phospho-IκBα (9246) and anti-IκBα (9242) antibodies were obtained from Cell Signaling Technology (Danvers, MA, USA). LPS (*Escherichia coli* serotype 055:B5) was from Sigma Chemical (St Louis, MO, USA).

Plasmids

The expression plasmid of STAT3C with mutations at A661C and N663C was kindly provided by J.E. Darnell (14). A dnSTAT3 vector carrying a mutation at Y705F was described previously (15). The human and mouse αCP-1 cDNAs were amplified by reverse transcription (RT)–PCR using primers human αCP-1: 5′-aagcttatggatgccggtgtg-3′ and 5′-gaattcgctgcaccccatgccctt-3′ and mouse αCP-1: 5′-gcggccgcatggacgccggtgtga-3′ and 5′-gtcgacctagctgcaccccat-3′, respectively. The cDNA was inserted into pCMV14 (Sigma Chemical) for FLAG-tag, pcDNA4 (Invitrogen, Carlsbad, CA, USA) for Myc-tag and pGEX-4T1 (Amersham Pharmacia Biotech, Piscataway, NJ, USA) for glutathione *S*-transferase (GST)-tag. The pMX-IRES-GFP and pGCDΔNsaI/E vectors were used for retroviral transduction (16). The psiRNA-hH1G2 or psiRNA-hH1 neo expression vector (Invivogen) was used for small interfering RNA (siRNA) knockdown (KD) experiments.

Retroviral constructs and transduction

pMX-STAT3C-IRES-GFP or pMX-dnSTAT3-IRES-GFP was retrovirally transduced in BMDCs according to the process presented in previous papers (17, 18). Briefly, PlatE, a packaging cell line, was transfected with pMX-STAT3C-IRES-GFP or pMX-dnSTAT3-IRES-GFP using FuGENE HD (Roche, Basel, Switzerland). GFP-positive PlatE cells were sorted by a cell sorter (FACSAria, BD Biosciences, San Jose, CA, USA). Stable virus producers were established by repeated sorting. The viruses were collected from the culture supernatants of the virus producers and used for the transduction of BMDCs. The mouse αCP-1-pGCDΔNsaI/E vector-containing IRES-GFP cassette was transfected into 293GPG-packaging cells as described previously (16). RAW264.7 cells were retrovirally transduced with the virus supernatants. Thirty-two hours later, GFP-positive cells (~40% GFP^+ cells) were sorted by a cell sorter and used for the assays.

Intracellular staining for cytokines and FACS

Retrovirally transduced BMDCs were stimulated with 10 ng ml^{-1} of LPS for 8 h in the presence of Brefeldin A (3 μg ml^{-1}, eBioscience, San Diego, CA, USA). The cells were stained with anti-CD11c–Allophycocyanin antibody (eBioscience), fixed and permeabilized using a Fixation and Permeabilization kit (eBioscience) followed by intracellular staining using anti-TNF-α–PE or anti-IL-6–PE antibodies (eBioscience). The cells were analyzed by a FACSCalibur (BD Biosciences).

Reporter gene analysis and EMSA

The NF-κB-responsive promoter luciferase reporter gene, a generous gift from T. Fujita (Laboratory of Molecular Genetics, Institute for Virus Research, Kyoto University, Japan), has been described (19). Reporter gene assay and Electrophoretic Mobility Shift Assay (EMSA) were performed as described previously (20, 21).

Immunoprecipitation assay, GST pull-down assay and western blot analysis

For immunoprecipitation, equal amounts of cellular proteins were incubated with anti-FLAG M2 affinity gel (Sigma Chemical) or protein G sepharose (Amersham Pharmacia Biotech) beads for 2 h at 4°C. The immunoprecipitates were collected by centrifugation and washed five times in washing buffer (1% NP-40 and 25 mM HEPES). Eluted samples were resolved by SDS–PAGE. The proteins were transferred to polyvinylidene difluoride membranes, and the membranes were immunoblotted with specific antibodies and visualized with appropriate HRP-conjugated secondary antibodies using the SuperSignal West Pico Chemiluminescent Substrate (Pierce Biotechnology, Rockford, IL, USA).

For GST pull-down assay, *E. coli* strain BL21 was transformed with human αCP-1-pGEX-4T1. GST and GST-αCP-1 proteins were purified by affinity chromatography. Transiently

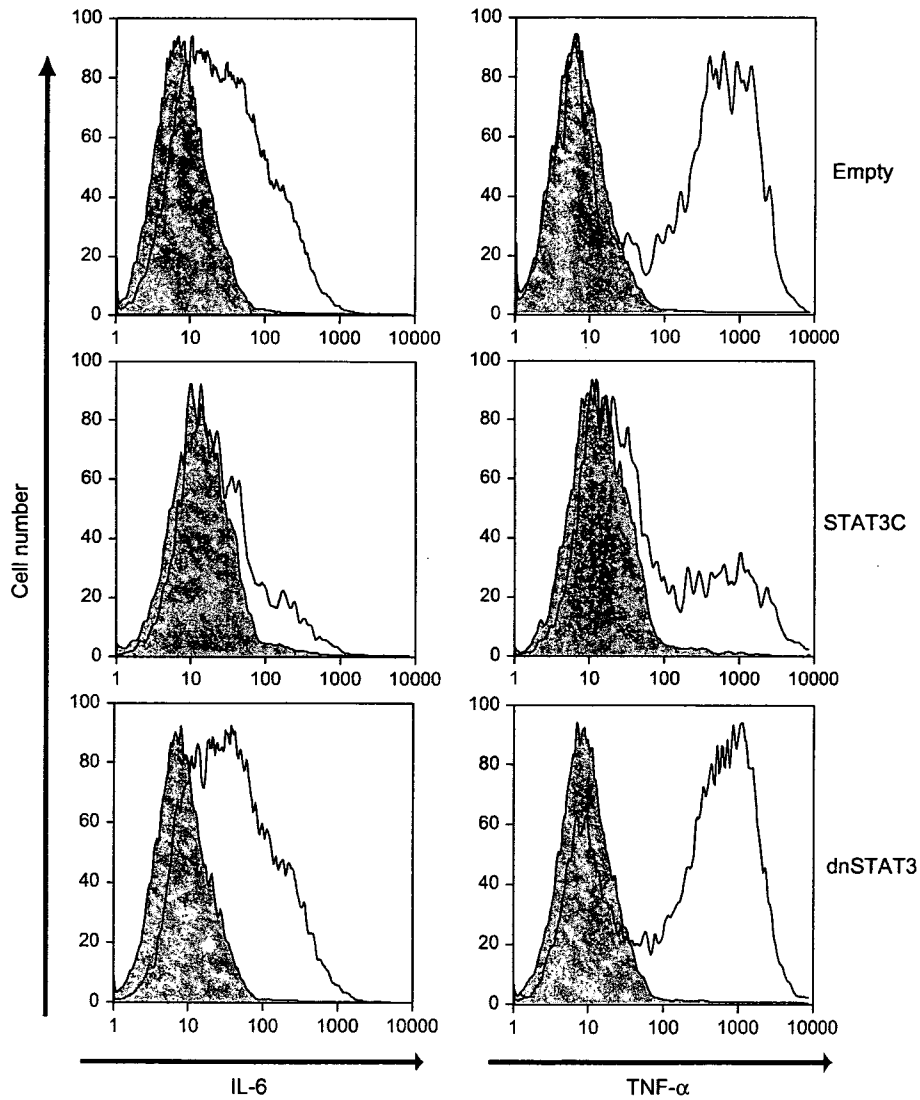

Fig. 1. Constitutive activation of STAT3 results in reduced LPS-induced IL-6 and TNF-α. BMDCs were retrovirally transduced with constitutively activated STAT3 (STAT3C)-IRES-GFP, dnSTAT3-IRES-GFP or an empty GFP vector. The BMDCs were left untreated (filled histogram) or stimulated with LPS (open histogram) for 8 h, followed by surface staining with an anti-CD11c antibody and intracellular staining with an anti-IL-6 or anti-TNF-α antibody. $CD11c^+$ GFP^+ cells were analyzed by FACS.

transfected HEK293T cells with FLAG-STAT3C plasmid were lysed and incubated with a purified control GST protein or GST-αCP-1 protein along with the suspension of glutathione–sepharose beads (Amersham Pharmacia Biotech) at 4°C for 2 h. The beads were washed and the precipitated proteins were analyzed by western blotting as previously described (22).

Preparation of nuclear extract, large-scale pull-down assay and mass spectrometric analysis

HEK293/TLR4 cells (1×10^7) were lysed in 5 ml of Buffer A [10 mM HEPES–HCl pH 7.9, 1.5 mM $MgCl_2$, 10 mM KCl, 1 mM dithiothreitol (DTT) and protease inhibitor cocktail (Nacalai Tesque, Kyoto, Japan)] on ice for 10 min. Then 10% NP-40 was added to a final concentration of 0.2%, and the mixture was vortexed for 10 sec and centrifuged at 10 000 r.p.m. for 1 min at 4°C. One milliliter volume of Buffer C [50 mM HEPES–HCl pH 7.9, 1.5 mM $MgCl_2$, 420 mM KCl, 1 mM EDTA, 20% glycerol, DTT (to 1 mM) and protease inhibitor cocktail] was added, and the pellets were left on ice for 30 min, vortexed for 10 sec and centrifuged at 15 000 r.p.m. for 10 min at 4°C. For the proteome-based analysis, the nuclear protein was incubated with anti-FLAG M2 affinity gel (Sigma Chemical) for 1 h at 4°C. The precipitated immune complexes were washed five times with washing buffer [0.25% NP-40 in Tris-buffered saline (TBS)], the bound proteins were eluted with FLAG peptide (Sigma Chemical) and the eluted fractions were concentrated with an Ultrafree-MC 10 000 NMW Filter Unit (Millipore, Billerica, MA, USA). The proteins were separated by SDS–PAGE and visualized by silver staining. For mass spectrometric analysis, proteins were cut from gels, digested with modified trypsin (sequencing grade, Promega, Madison, WI, USA) (23) and loaded into an automated nanoflow liquid chromatography system for tandem mass spectrometry (Finnigan LCQ Deca, Thermo Fisher Scientific, Waltham, MA, USA). The peptide masses obtained by LC-MS/MS analysis were searched against the non-redundant

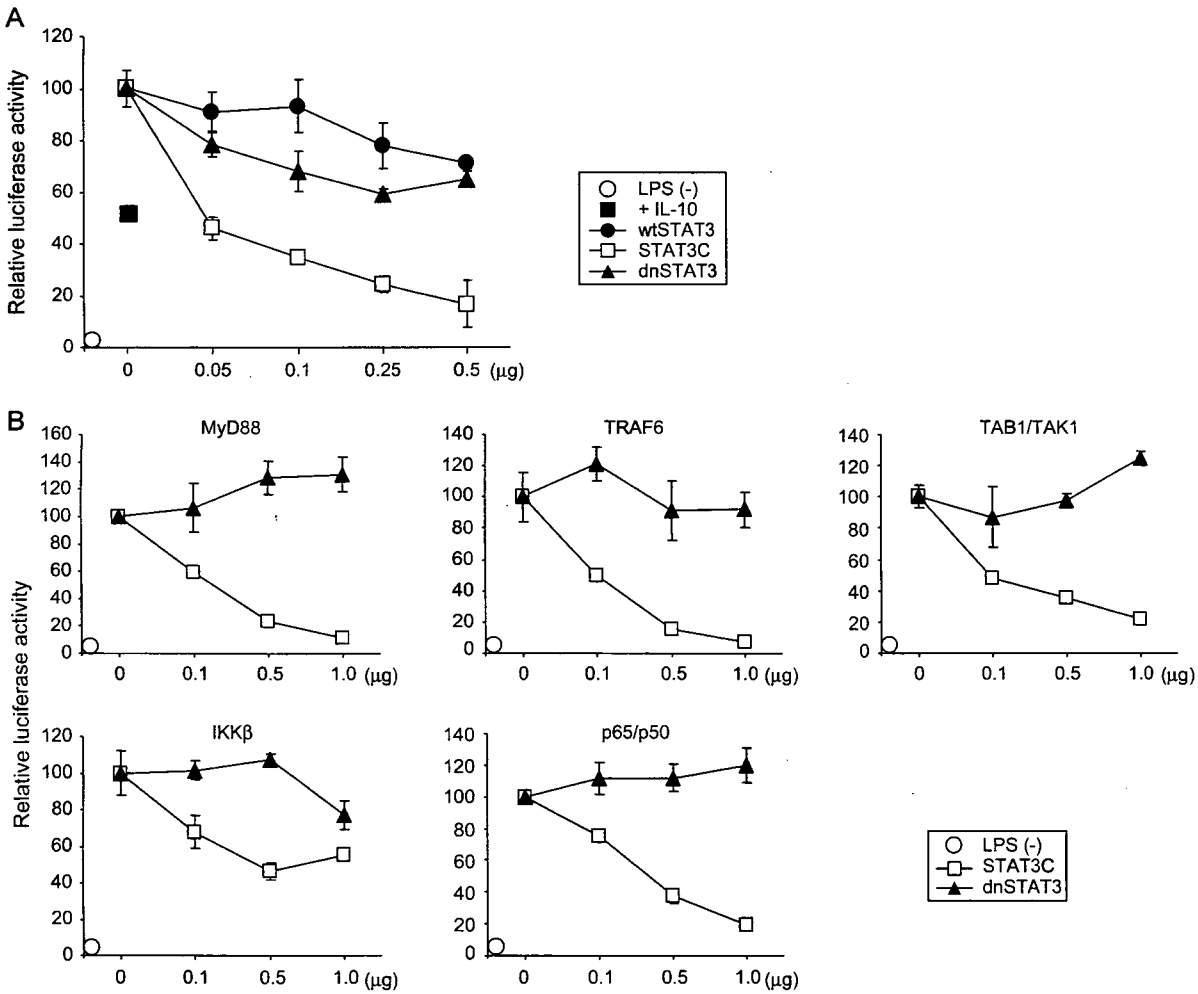

Fig. 2. STAT3C suppresses the LPS-induced activation of NF-κB. (A) The indicated amounts of wild-type STAT3, STAT3C and dnSTAT3 cDNA were transfected into HEK293/TLR4 cells along with an NF-κB luciferase reporter. Twenty-four hours later, the cells were pre-treated with IL-10 stimulated with LPS, and then luciferase activity was measured and normalized based on β-galactosidase activity. (B) HEK293T cells were transfected with the indicated amount of STAT3C or dnSTAT3 together with an NF-κB luciferase reporter and MyD88, TRAF6, TAB1/TAK1, IKKβ or p65/p50 cDNA. Luciferase activity was determined as described in (A). Means ± SD of triplicate samples of one representative experiment out of three independent experiments are shown.

protein sequence database of the National Center for Biotechnology Information using the Mascot search engine (Matrix Science, Boston, MA, USA).

Measurement of cytokines

mRNA expression levels and protein levels for IL-6 and TNF-α were determined by RT–PCR and ELISA (eBioscience) as described previously (24, 25).

Generation of mouse αCP-1 KD cells

siRNA sequences that target the human αCP-1 position at 991 bp (5′-ggctctgctgccagtattagt-3′) and the mouse αCP-1 position at 11 bp (5′-gtgtgactgaaagcggactca-3′) were determined by Invivogen siRNA Wizard software. The annealed nucleotides were inserted into the psiRNA-hH1G2 or psiRNA-hH1 neo expression vector. RAW264.7 cells were transfected with the control or psiRNA-hH1neo-αCP-1 vector using FuGENE HD. Stable RAW264.7 cell transformants were selected with 0.8 mg ml^{-1} of G418 (26). Several G418-resistant clones were isolated and assayed.

RNA co-immunoprecipitation assay

RAW264.7 cells were untreated or stimulated with LPS (100 ng ml^{-1}) for 3 h. Then the cells were lysed with the lysis buffer (20 mM HEPES pH 7.4, 150 mM NaCl, 12.5 mM β-glycerophosphate, 1.5 mM $MgCl_2$, 2 mM EGTA, 10 mM NaF, 2 mM DTT, 1 mM Na_3VO_4, 1 mM phenylmethylsulphonylfluoride, 20 μM aprotinin and 0.5% Triton X-100), and the cell lysates were incubated with anti-αCP-1 antibody, control goat IgG or no antibody for 30 min at 4°C, followed by 45 min of further incubation along with protein G sepharose beads. The beads were washed with TBS containing 0.05% Tween 20, re-suspended with 20 μl of the same buffer and boiled for 5 min. The supernatants were subjected to RT–PCR as described previously (24, 25).

Results

STAT3C suppresses NF-κB activity without any effects on signal transduction in LPS signaling

Although STAT3 is indispensable for IL-10 function, it is still unclear whether STAT3 activation is sufficient for the suppression of pro-inflammatory cytokines. We first examined the effect of STAT3C, a constitutively activated form of STAT3, on LPS-induced IL-6 and TNF-α production in BMDCs. The over-expression of STAT3C, but not an empty control or dnSTAT3, suppressed the protein production of IL-6 and TNF-α (Fig. 1). This result suggests that activated STAT3 is sufficient for the suppression of pro-inflammatory cytokine production in BMDCs.

Then we examined whether the over-expression of STAT3C in HEK293/TLR4 cells is sufficient for the suppression of NF-κB transcriptional activity (Fig. 2A). STAT3C, but neither wild-type STAT3 nor dnSTAT3, suppressed LPS–TLR4-mediated NF-κB reporter activation. The suppressive effect of STAT3C was even greater than that of IL-10 (Fig. 2A). The inhibitory effect of STAT3C on NF-κB activation was also observed in the cells in which NF-κB was activated by the forced expression of signaling molecules downstream of TLR4, such as MyD88, TRAF6, TAB1/TAK1, IKKβ and the heterodimeric complex of NF-κB subunits, p65/p50 (Fig. 2B). The inhibitory effect of STAT3C was not non-specific transcriptional repression since STAT3C enhanced APRE reporter promoter activity (data not shown). This result suggests that STAT3C inhibits NF-κB transcriptional activity but not signaling intermediates.

To investigate this possibility further, we examined the effects of STAT3C on the activation of signaling molecules involved in LPS signaling. HEK293/TLR4 cells were transfected with either STAT3C or an empty vector and then stimulated with LPS. The phosphorylation of IκBα, ERK, p38 and JNK, as well as the degradation of IκBα, was measured by western blotting (Fig. 3A). Similar activation of MAPKs, as well as IκBα phosphorylation and degradation, was observed between empty and STAT3C vector transfected cells. Furthermore, EMSA assay revealed that DNA-binding activity of NF-κB was similarly activated by LPS in the presence or absence of STAT3C (Fig. 3B). These results suggest that STAT3C does not affect proximal signaling events of TLR4, including the DNA-binding activity of NF-κB, but rather affects the transcriptional activity of NF-κB.

Identification of αCP-1 as a STAT3C-binding protein

To define the molecular mechanism of transcriptional repression by STAT3C, we first examined the direct interaction between STAT3C and NF-κB subunits. We could not show direct co-immunoprecipitation of STAT3C with a p65 subunit of NF-κB (data not shown). STAT3 has been shown to interact

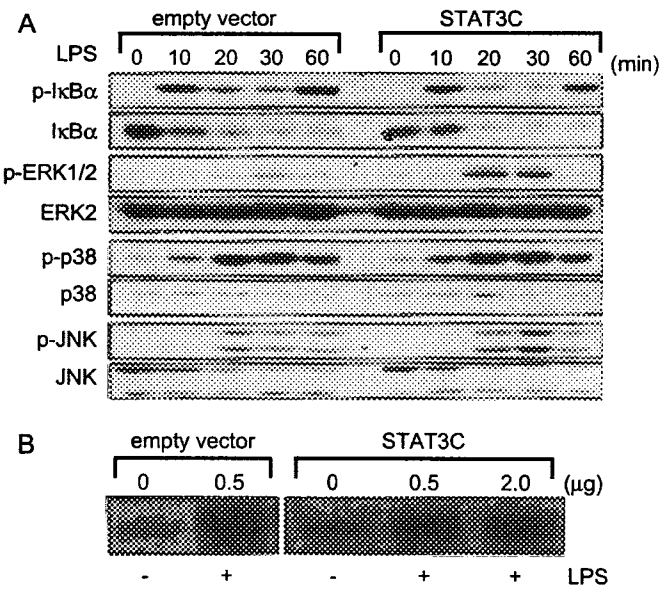

Fig. 3. STAT3C does not affect LPS signaling. (A) HEK293/TLR4 cells were transfected with an empty vector or STAT3C and then stimulated with LPS. The cells were harvested and lysed at the indicated time points. Western blot analysis was performed with the indicated antibodies. One representative experiment out of three independent experiments is shown. (B) HEK293/TLR4 cells were transfected with the indicated amount of empty vector or STAT3C and then stimulated with LPS for 30 min. The NF-κB DNA-binding activity in nuclear extracts was determined by EMSA. One representative experiment out of two independent experiments is shown.

with transcriptional co-activator p300 (27). Thus, we examined the effect of the over-expression of p300 to examine the possibility of sequestration of p300 by STAT3C. However, the over-expression of p300 did not reverse the suppressive effect of STAT3C (data not shown). Because transcriptional repression is often mediated by co-repressor complexes with histone deacetylase (HDAC) activity, we examined the effect of various HDAC inhibitors. However, none of the HDAC inhibitors reversed the effect of STAT3C (data not shown), leading us to suspect that STAT3C recruits a novel transcriptional/translational repressor.

To identify the proteins interacting with STAT3C, FLAG-STAT3C was over-expressed in HEK293/TLR4 cells and immunoprecipitated with FLAG M2 beads from nuclear extracts. The proteins eluted were resolved by SDS–PAGE and then visualized with silver staining (Fig. 4A). The bands co-precipitated with STAT3C were identified using automated nanoflow liquid chromatography. Among several proteins identified, an ~40 kDa protein was identified as αCP-1 [hnRNP E1 and poly(C)-binding protein (PCBP)-1] by tryptic fragmentation and subsequent MS/MS analysis (Fig. 4B). We further characterized this molecule because αCP-1 is reported to suppress the expression of several genes (28, 29).

The αCP-1 is a K-homology domain containing an RNA-binding protein and a member of the PCBP family, which consists of five PCBPs (αCP-1-4 and hnRNP K). First, we confirmed that αCP-1 was constitutively expressed in the cytoplasm and nucleus and was not induced by IL-10 (data not shown). We obtained the full-length αCP-1 cDNA by RT–PCR and sub-cloned it into an expression vector. Then we

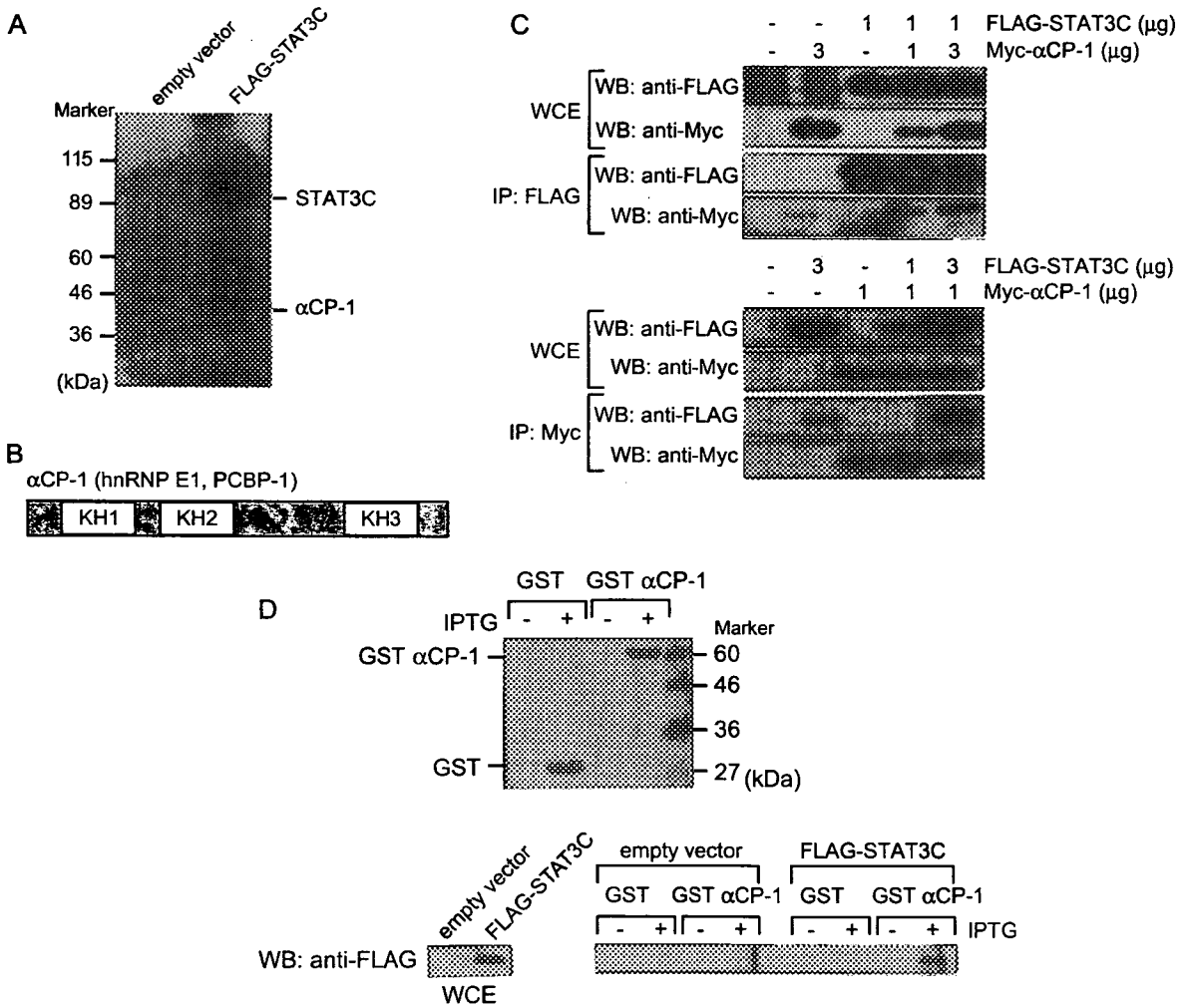

Fig. 4. STAT3C interacts with an RNA-binding protein, αCP-1. (A) HEK293/TLR4 cells were transfected with empty or FLAG-STAT3C plasmid. Thirty-six hours later, the cells were lysed and dissolved by SDS–PAGE. The silver staining of the gel is shown. Distinct bands in the STAT3C-transfected, LPS-stimulated condition were subjected to LC-ESI-MS/MS mass spectrometric analysis. The locations of STAT3C and αCP-1 are indicated. (B) A schematic diagram of the αCP-1 protein. KH represents the K-homology domain. (C) HEK293T cells were transfected with FLAG-STAT3C and Myc-αCP-1 vectors. Twenty-four hours later, the whole-cell extracts (WCE) were immunoprecipitated (IP) with anti-FLAG or anti-Myc antibody and blotted with antibodies as indicated (WB). (D) GST-αCP-1 fusion protein was expressed in BL21 *Escherichia coli*, extracted and visualized by Coomassie brilliant blue staining (upper panel). The WCE from HEK293T cells transfected with FLAG-STAT3C or an empty vector (lower left panel) were incubated with control GST or GST-αCP-1, precipitated with glutathione–sepharose beads and blotted with anti-FLAG antibody (lower right panel).

confirmed the interaction between STAT3C and αCP-1 by the co-immunoprecipitation assay (Fig. 4C). When FLAG-tagged STAT3C and Myc-tagged αCP-1 were expressed in HEK293T cells, STAT3C and αCP-1 were clearly co-immunoprecipitated with opponent antibodies. Furthermore, we confirmed the interaction between STAT3C and GST-αCP-1 *in vitro* using recombinant GST-αCP-1 (Fig. 4D). Purified GST-αCP-1 beads were incubated with HEK293T cell extracts containing FLAG-STAT3C. As shown in Fig. 4(D), GST-αCP-1, but not GST, precipitated STAT3C. These data indicate that αCP-1 physically interacted with STAT3C.

Role of αCP-1 in LPS-induced NF-κB activation

To examine the effect of αCP-1 on LPS-mediated NF-κB activation, we over-expressed various amounts of αCP-1 and STAT3C in HEK293/TLR4 cells. As shown in Fig. 5(A), αCP-1 alone suppressed LPS-induced NF-κB activity in a dose-dependent manner. Moreover, when αCP-1 and STAT3C were simultaneously expressed in HEK293/TLR4 cells, further suppression of NF-κB activity was observed.

Next, we examined the effect of the reduced expression of endogenous αCP-1 by siRNA. The siRNA expression reduced the level of αCP-1 mRNA (data not shown) and partly reversed NF-κB repression by STAT3C (Fig. 5B). These results suggest that αCP-1 is involved in the STAT3-mediated suppression of LPS-induced NF-κB activation. αCP-1, in particular, could be a partial transcriptional repressor of NF-κB because of its suppressive effect on NF-κB transcriptional activity.

Effect of forced expression of αCP-1 on LPS-induced pro-inflammatory cytokines

To elucidate the *in vitro* function of αCP-1 in the context of pro-inflammatory cytokine induction in macrophages, we first generated macrophage-like cells expressing elevated levels of αCP-1. RAW264.7 cells were transduced with αCP-1-IRES-GFP or a control GFP retrovirus vector, and the GFP-positive fraction was sorted by FACS. As shown in Fig. 6(A), an ~2-fold increase in αCP-1 expression levels was detected by western blotting with anti-αCP-1 antibody in αCP-1-transduced cells. In our condition, IL-6 was slightly produced in RAW264.7 cells infected with an empty vector without LPS stimulation, and IL-10 had little effect on the basal level of IL-6 production in the cells (Fig. 6B). IL-10 strongly reduced the LPS-induced production of IL-6 and TNF-α in the cells with the empty vector. Although LPS-induced IL-6 levels were similar between the cells infected with empty and αCP-1 vectors, IL-10 suppressed LPS-induced IL-6 production more profoundly in the cells with αCP-1. Thus, the suppressive effect of IL-10 on IL-6 was significantly enhanced by the forced expression of αCP-1. However, the forced expression of αCP-1 did not affect IL-10-mediated TNF-α suppression (Fig. 6B), indicating an IL-6-specific manner.

To further confirm the role of αCP-1 in the suppressive effect of IL-10 on IL-6 production, we investigated the mRNA expression of IL-6 in the RAW264.7 cells infected with an empty or αCP-1 vector. As shown in Fig. 6(C), the elevation of IL-6 mRNA levels by LPS was suppressed in IL-10 pre-treated cells infected with an empty vector. The reduction of IL-6 mRNA levels by IL-10 was prominent in the cells infected with αCP-1 and showed no effect on the kinetics (Fig. 6C). In contrast, the reduction of TNF-α mRNA levels by IL-10 was not affected by αCP-1 (data not shown). These results suggest that αCP-1 is involved in the IL-10–STAT3-mediated reduction of mRNA levels of pro-inflammatory cytokine, particularly IL-6, but not TNF-α.

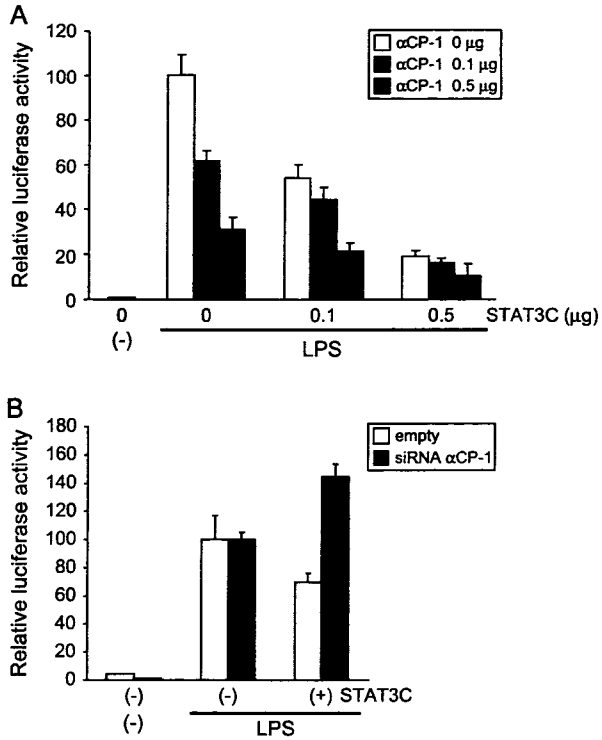

Fig. 5. αCP-1 suppresses LPS-induced NF-κB activation. (A) HEK293/TLR4 cells were transfected with the indicated amounts of STAT3C, αCP-1 or both cDNA and an NF-κB luciferase reporter. Twenty-four hours later, the cells were stimulated with LPS for 6 h, and then luciferase activities were measured. Means ± SD of triplicate samples of one representative experiment out of three independent experiments are shown. (B) HEK293/TLR4 cells were transfected with STAT3C, siRNA-αCP-1 or an empty vector along with an NF-κB luciferase reporter. Luciferase activity was determined as described in (A).

Effect of the knockdown of αCP-1 on LPS-induced pro-inflammatory cytokines

In order to confirm the role of αCP-1 in suppressing IL-6 production in macrophages, we established several αCP-1-KD RAW264.7 cell clones. As shown in Fig. 7(A), the expression levels were decreased by ~50% in the KD cell line, clone KD-1, compared with the endogenous αCP-1 level. Consistent with the results shown in Fig. 6(B), IL-6 was slightly produced in the clone with the empty vector without LPS stimulation, and IL-10 had little effect on the basal level of IL-6 production in the cells (Fig. 7B). The basal level of IL-6 in KD-1 was slightly increased by IL-10 treatment. As expected, the suppressive effect of IL-10 on IL-6 secretion was attenuated significantly in KD-1. Similar results were also observed in the different clones (data not shown). On the other hand, the ratio of suppression of TNF-α production

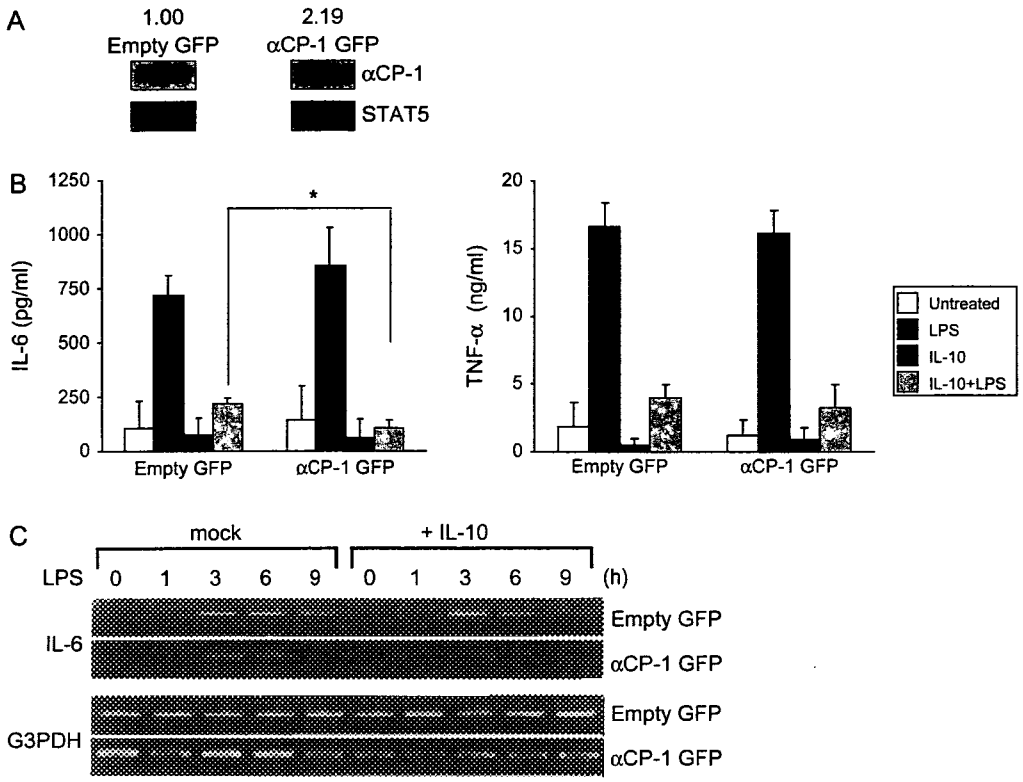

Fig. 6. Forced expression of αCP-1 enhances the suppressive effect of IL-10 on LPS-induced IL-6 production. (A–C) RAW264.7 cells were retrovirally transduced with empty GFP or αCP-1 GFP, and the GFP-positive cells were sorted. (A) The whole-cell extracts were analyzed by western blotting with the indicated antibodies. The relative intensities of each αCP-1 band normalized by STAT5 expression levels are shown above. (B and C) Retrovirally transduced RAW264.7 cells were pre-treated with IL-10 for 30 min and then stimulated with LPS for 12 h (B) or for the indicated times (C). The concentrations of IL-6 and TNF-α in the culture supernatants were measured by ELISA (B). Asterisk indicates statistically significant differences between the groups ($P < 0.005$). The IL-6 mRNA was analyzed by RT-PCR (C).

by IL-10 (~80% suppression) was comparable between the control clone and KD-1 (Fig. 7B). Interestingly, TNF-α production by LPS was enhanced in KD-1 (Fig. 7B).

A reduced IL-10 effect was also confirmed by RT–PCR. As shown in Fig. 7(C), IL-10 failed to suppress IL-6 mRNA expression in KD-1, especially at 3 h stimulation. However, there was no difference in the TNF-α mRNA levels of the control and KD-1 cells (data not shown). These findings further support a strong link between the αCP-1 and IL-10–STAT3-mediated suppression of IL-6.

Selective interaction between αCP-1 protein and IL-6 mRNA

αCP-1 is a member of the PCBP family, which interacts with RNA. Thus, we investigated whether the αCP-1 protein can bind to pro-inflammatory cytokine mRNA. RAW264.7 cells were stimulated with or without LPS, and then the αCP-1 protein was immunoprecipitated with an anti-αCP-1 antibody. IL-6 or TNF-α mRNA was detected by RT–PCR using RNA co-immunoprecipitated with an anti-αCP-1 antibody as a template. As shown in Fig. 8, IL-6 mRNA, but not TNF-α mRNA, was detected in the anti-αCP-1 antibody immunoprecipitates. These results suggest that the αCP-1 protein selectively binds to IL-6 mRNA but not to TNF-α mRNA, which may account for the suppressive effect of αCP-1 on IL-6 but not on TNF-α, as shown in Figs. 6 and 7.

Discussion

The IL-10–STAT3-signaling pathway plays a critical role in anti-inflammatory effects on the immune system. For example, IL-10-deficient mice as well as conditional knockout mice deficient for STAT3 in APCs show the spontaneous development of chronic enterocolitis (7, 30). IL-10 strongly suppresses various aspects of inflammatory responses induced by LPS on APCs, such as macrophages and dendritic cells. While the signaling pathways emanated from TLR to activate APCs are well characterized, the mechanism by which IL-10 suppresses TLR-mediated NF-κB activation is poorly understood. Numerous groups have searched for the IL-10-regulated genes responsible for the anti-inflammatory effect because anti-inflammatory effects of IL-10 has been shown to require *de novo* protein synthesis. However, none of the target genes has been able to replace the anti-inflammatory effect of IL-10 alone. For example, the over-expression of Bcl-3, an IL-10-inducible gene, inhibits LPS-induced TNF-α production, but IL-10 still shows the suppression of IL-6 production in macrophages lacking Bcl-3 (5). Bcl-3 is shown to interact with NF-κB p50 subunit, which may interfere with the recruitment of the NF-κB, p65/p50 heterodimer to the TNF-α promoter. On the other hand, the over-expression of IκBNS, an IL-10-dependent colonic lamina propria macrophage-specific gene, inhibits LPS-induced IL-6 production

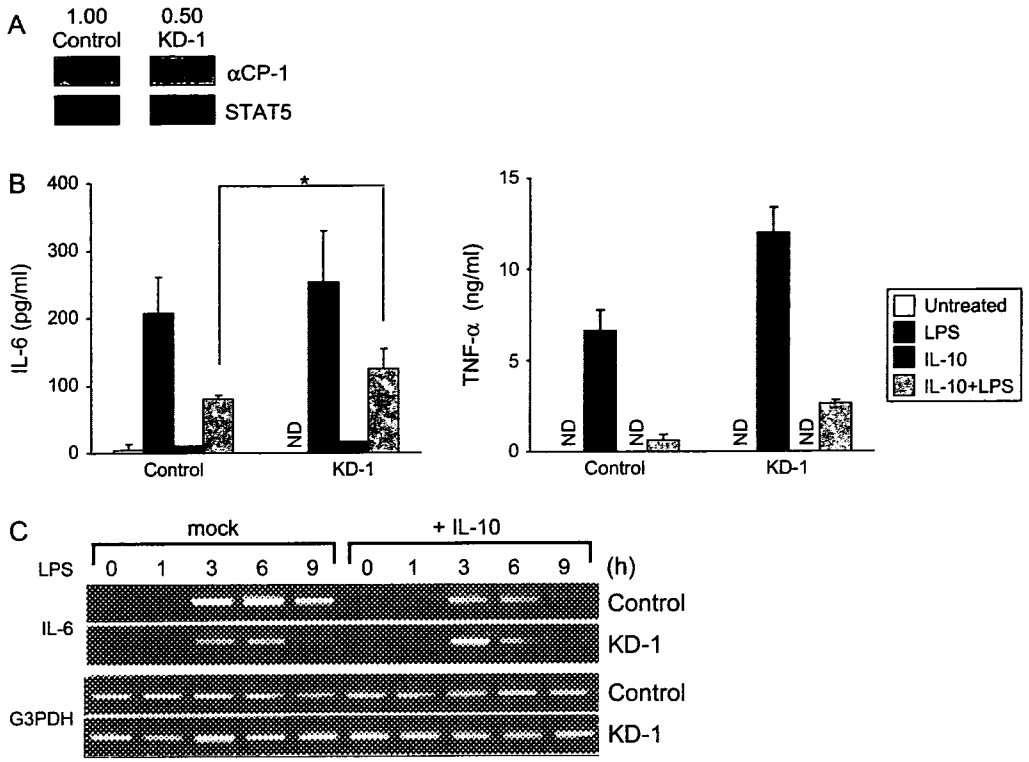

Fig. 7. Knockdown of αCP-1 cancels the suppressive effect of IL-10 on LPS-induced IL-6 production. (A–C) The expression of αCP-1 was down-regulated by siRNA in RAW264.7 cells. (A) The whole-cell extracts from RAW264.7 cells transfected with the control vector (control) and an αCP-1 KD clone (KD-1) were analyzed by western blotting with the indicated antibodies. The relative intensities of each αCP-1 band normalized by STAT5 expression levels are shown above. (B and C) Control and KD-1 RAW264.7 cells were pre-treated with IL-10 for 30 min and then stimulated with LPS for 12 h (B) or for the indicated times (C). The concentrations of IL-6 and TNF-α in the culture supernatants were measured by ELISA (B). Asterisk indicates statistically significant differences between the groups ($P < 0.005$). The IL-6 mRNA was analyzed by RT–PCR (C).

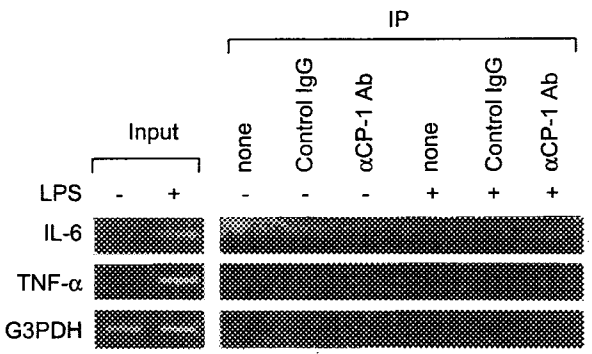

Fig. 8. αCP-1 protein binds to IL-6 mRNA but not to TNF-α mRNA. RAW264.7 cells were untreated (–) or treated with LPS for 3 h (+) and then lysed. IL-6, TNF-α and G3PDH Glyceraldehyde-3-phosphate dehydrogenase mRNAs were amplified by RT–PCR using the lysates of whole-cell extracts (input) or the lysates of immunoprecipitates (IP) with an anti-αCP-1 antibody, control goat IgG or no antibody (none) along with protein G sepharose beads.

but not TNF-α production (31). Therefore, it is possible that anti-inflammatory effects of IL-10 could be a sum of the effects of IL-10-inducible, anti-inflammatory genes.

In addition, we suspected that activated STAT3 itself may have an anti-inflammatory effect because we and others have demonstrated that the prolonged activation of STAT3 is necessary to elicit an anti-inflammatory effect (9, 10). To further demonstrate this notion, we examined whether STAT3C, a constitutively activated form of STAT3, directly suppresses TLR4 signaling and NF-κB activity. We have clearly demonstrated that STAT3 can directly suppress NF-κB transcriptional activity without affecting the signal transduction pathways of TLR4. We then hypothesized that a novel factor associated with STAT3C links STAT3 activation to NF-κB suppression.

To evaluate this hypothesis, we sought the factors associated with STAT3C and found an RNA-binding protein, αCP-1. In this study, we propose that this novel STAT3C-binding protein, αCP-1, is involved in the IL-10–STAT3-mediated suppression of NF-κB activation. αCPs have been implicated in a wide range of post-transcriptional regulatory pathways, including not only mRNA stabilization but also translation silencing (32, 33). hnRNP K has been reported to directly interact *in vitro* and *in vivo* with zinc finger transcriptional repressor Zik-1 and with other structurally related transcriptional repressors such as Kid-1 and MZF-1 (32). Since αCP-1 over-expression with STAT3C suppressed NF-κB reporter gene activity (Fig. 5), αCP-1 may directly or indirectly inhibit NF-κB transcriptional activity. Thus, αCP-1 may function as a transcriptional repressor. However, the molecular mechanism for this function is unclear at present.

We found that αCP-1 bound to IL-6 mRNA but not to TNF-α mRNA (Fig. 8), which may explain why the effect of αCP-1

is stronger for IL-6 than for TNF-α (Figs 6 and 7). Although αCP-1 has been shown to stabilize certain mRNAs by binding to a 3′-untranslated region C-rich motif (33), this mechanism is not at work the case because the forced expression of αCP-1 reduced the mRNA levels of IL-6 in RAW264.7 cells treated with IL-10 (Fig. 6C). The MAPK, p38 pathway, mediates the stabilization of TNF-α mRNA via HuR and Tristetraprolin (TTP) in myeloid cells stimulated with LPS (6, 34). One of the effects of IL-10 is the destabilization of the mRNA of TNF-α by the suppression of p38 activation and the inhibition of HuR expression (6). There is a possibility that αCP-1 interacts with IL-6 mRNA 3′-untranslated region and blocks stabilization by HuR and TTP. However, we did not see any differences in IL-6 mRNA stability by the forced expression of αCP-1 (data not shown). Thus, αCP-1 may affect the transcription, splicing or nuclear transport, rather than the stability, of IL-6 mRNA.

αCP-1 may affect translation. αCP-1, αCP-2 and hnRNP K were shown to specifically and efficiently inhibit the translation of the HPV-16 L2 mRNA *in vitro* (35). αCP-2 has been shown to inhibit the translation of CCAAT/enhancer binding protein α mRNA, which leads to the suppression of the expression of C/EBPα and G-CSF-R and leads to rapid cell death in the breakpoint cluster region-Abelson-expressing myeloid cells (36). It has also been shown that hnRNP K and αCP-1 induce the translational silencing of 15-lipoxygenase (37). Thus, STAT3–αCP-1 may suppress the translation of pro-inflammatory genes, particularly IL-6, in addition to transcriptional repression. Further investigation is necessary to reveal the precise mechanisms suppressing IL-6 transcription by STAT3–αCP-1. A comprehensive analysis using microarray is required to identify other genes regulated by αCP-1. In addition, the loss or gain of function analysis of αCP-1 *in vivo* using animal models is critical to clarify the physiological role of this molecule.

Our data provide a novel mechanism employing αCP-1 for the IL-10–STAT3-mediated suppression of NF-κB activation and IL-6 production. Therefore, the up-regulation of αCP-1 may represent a potential therapeutic pathway for the treatment of inflammatory diseases by enhancing the effect of IL-10.

Acknowledgements

We thank Yuuki Kawabata and Tomoko Yoshioka for general assistance. Emiko Fujimoto and Masumi Ohtsu (Technical Support Center, Medical Institute of Bioregulation) for conducting mass spectrometry and DNA sequencing, Makoto Matsumoto (Hyogo College Of Medicine) for EMSA assay and Yukiko Nishi for preparing the manuscript. This work was supported by special grants-in-aid from the Ministry of Education, Science, Technology, Sports and Culture of Japan and from the Japan Diabetes Foundation, the Uehara Memorial Foundation, the Kato Memorial Bioscience Foundation, the Takeda Science Foundation and the Haraguchi Memorial Foundation.

Abbreviations

APC	antigen-presenting cell
Bcl-3	B cell lymphoma-3
BMDC	bone marrow-derived dendritic cell
C/EBPα	CCAAT/enhancer binding protein α
dnSTAT3	dominant-negative form of signal transducer and activator of transcription 3
DTT	dithiothreitol
EMSA	electrophoretic mobility shift assay
ERK	extracellular signal-regulated kinase
G3PDH	glyceraldehyde-3-phosphate dehydrogenase
GST	glutathione *S*-transferase
HDAC	histone deacetylase
IκBα	inhibitory nuclear factor-κBα
IPTG	isopropyl β-D-thiogalactoside
JNK	c-Jun N-terminal kinase
KD	knockdown
MAPK	mitogen-activated protein kinase
NF-κB	nuclear factor-κB
PCBP	poly(C)-binding protein
RT	reverse transcription
siRNA	small interfering RNA
SOCS3	suppressor of cytokine signaling 3
STAT3	signal transducer and activator of transcription 3
TBS	Tris-buffered saline
TLR	Toll-like receptor
TNF-α	tumor necrosis factor-α
TTP	Tristetraprolin

References

1 Moore, K. W., de Waal Malefyt, R., Coffman, R. L. and O'Garra, A. 2001. Interleukin-10 and the interleukin-10 receptor. *Annu. Rev. Immunol.* 19:683.
2 Lee, T. S. and Chau, L. Y. 2002. Heme oxygenase-1 mediates the anti-inflammatory effect of interleukin-10 in mice. *Nat. Med.* 8:240.
3 Schottelius, A. J., Mayo, M. W., Sartor, R. B. and Baldwin, A. S. Jr 1999. Interleukin-10 signaling blocks inhibitor of kappaB kinase activity and nuclear factor kappaB DNA binding. *J. Biol. Chem.* 274:31868.
4 Bhattacharyya, S., Sen, P., Wallet, M., Long, B., Baldwin, A. S. Jr and Tisch, R. 2004. Immunoregulation of dendritic cells by IL-10 is mediated through suppression of the PI3K/Akt pathway and of IkappaB kinase activity. *Blood* 104:1100.
5 Kuwata, H., Watanabe, Y., Miyoshi, H. *et al.* 2003. IL-10-inducible Bcl-3 negatively regulates LPS-induced TNF-alpha production in macrophages. *Blood* 102:4123.
6 Rajasingh, J., Bord, E., Luedemann, C. *et al.* 2006. IL-10-induced TNF-alpha mRNA destabilization is mediated via IL-10 suppression of p38 MAP kinase activation and inhibition of HuR expression. *FASEB J.* 20:2112.
7 Takeda, K., Clausen, B. E., Kaisho, T. *et al.* 1999. Enhanced Th1 activity and development of chronic enterocolitis in mice devoid of Stat3 in macrophages and neutrophils. *Immunity* 10:39.
8 Williams, L., Bradley, L., Smith, A. and Foxwell, B. 2004. Signal transducer and activator of transcription 3 is the dominant mediator of the anti-inflammatory effects of IL-10 in human macrophages. *J. Immunol.* 172:567.
9 Yasukawa, H., Ohishi, M., Mori, H. *et al.* 2003. IL-6 induces an anti-inflammatory response in the absence of SOCS3 in macrophages. *Nat. Immunol.* 4:551.
10 El Kasmi, K. C., Holst, J., Coffre, M. *et al.* 2006. General nature of the STAT3-activated anti-inflammatory response. *J. Immunol.* 177:7880.
11 Wang, T., Niu, G., Kortylewski, M. *et al.* 2004. Regulation of the innate and adaptive immune responses by Stat-3 signaling in tumor cells. *Nat. Med.* 10:48.
12 Butcher, B. A., Kim, L., Panopoulos, A. D., Watowich, S. S., Murray, P. J. and Denkers, E. Y. 2005. IL-10-independent STAT3 activation by *Toxoplasma gondii* mediates suppression of IL-12 and TNF-alpha in host macrophages. *J. Immunol.* 174:3148.
13 Hanada, T., Tanaka, K., Matsumura, Y. *et al.* 2005. Induction of hyper Th1 cell-type immune responses by dendritic cells lacking the suppressor of cytokine signaling-1 gene. *J. Immunol.* 174:4325.
14 Bromberg, J. F., Wrzeszczynska, M. H., Devgan, G. *et al.* 1999. Stat3 as an oncogene. *Cell* 98:295.
15 Nakajima, K., Yamanaka, Y., Nakae, K. *et al.* 1996. A central role for Stat3 in IL-6-induced regulation of growth and differentiation in M1 leukemia cells. *EMBO J.* 15:3651.

16 Suzuki, A., Obi, K., Urabe, T. *et al.* 2002. Feasibility of *ex vivo* gene therapy for neurological disorders using the new retroviral vector GCDNsap packaged in the vesicular stomatitis virus G protein. *J. Neurochem.* 82:953.
17 Kinjyo, I., Inoue, H., Hamano, S. *et al.* 2006. Loss of SOCS3 in T helper cells resulted in reduced immune responses and hyperproduction of interleukin 10 and transforming growth factor-beta 1. *J. Exp. Med.* 203:1021.
18 Morita, S., Kojima, T. and Kitamura, T. 2000. Plat-E: an efficient and stable system for transient packaging of retroviruses. *Gene Ther.* 7:1063.
19 Fujita, T., Nolan, G. P., Liou, H. C., Scott, M. L. and Baltimore, D. 1993. The candidate proto-oncogene bcl-3 encodes a transcriptional coactivator that activates through NF-kappa B p50 homodimers. *Genes Dev.* 7:1354.
20 Minoda, Y., Saeki, K., Aki, D. *et al.* 2006. A novel Zinc finger protein, ZCCHC11, interacts with TIFA and modulates TLR signaling. *Biochem. Biophys. Res. Commun.* 344:1023.
21 Kuwata, H., Matsumoto, M., Atarashi, K. *et al.* 2006. IkappaBNS inhibits induction of a subset of Toll-like receptor-dependent genes and limits inflammation. *Immunity* 24:41.
22 Mashima, R., Saeki, K., Aki, D. *et al.* 2005. FLN29, a novel interferon- and LPS-inducible gene acting as a negative regulator of toll-like receptor signaling. *J. Biol. Chem.* 280:41289.
23 Saeki, K., Miura, Y., Aki, D., Kurosaki, T. and Yoshimura, A. 2003. The B cell-specific major raft protein, Raftlin, is necessary for the integrity of lipid raft and BCR signal transduction. *EMBO J.* 22:3015.
24 Chinen, T., Kobayashi, T., Ogata, H. *et al.* 2006. Suppressor of cytokine signaling-1 regulates inflammatory bowel disease in which both IFNgamma and IL-4 are involved. *Gastroenterology* 130:373.
25 Aki, D., Mashima, R., Saeki, K., Minoda, Y., Yamauchi, M. and Yoshimura, A. 2005. Modulation of TLR signalling by the C-terminal Src kinase (Csk) in macrophages. *Genes Cells* 10:357.
26 Kinjyo, I., Hanada, T., Inagaki-Ohara, K. *et al.* 2002. SOCS1/JAB is a negative regulator of LPS-induced macrophage activation. *Immunity* 17:583.
27 Yuan, Z. L., Guan, Y. J., Chatterjee, D. and Chin, Y. E. 2005. Stat3 dimerization regulated by reversible acetylation of a single lysine residue. *Science* 307:269.
28 Paulding, W. R. and Czyzyk-Krzeska, M. F. 1999. Regulation of tyrosine hydroxylase mRNA stability by protein-binding, pyrimidine-rich sequence in the 3′-untranslated region. *J. Biol. Chem.* 274:2532.
29 Rivera-Gines, A., Cook, R. J., Loh, H. H. and Ko, J. L. 2006. Interplay of Sps and poly(C) binding protein 1 on the mu-opioid receptor gene expression. *Biochem. Biophys. Res. Commun.* 345:530.
30 Kuhn, R., Lohler, J., Rennick, D., Rajewsky, K. and Muller, W. 1993. Interleukin-10-deficient mice develop chronic enterocolitis. *Cell* 75:263.
31 Hirotani, T., Lee, P. Y., Kuwata, H. *et al.* 2005. The nuclear IkappaB protein IkappaBNS selectively inhibits lipopolysaccharide-induced IL-6 production in macrophages of the colonic lamina propria. *J. Immunol.* 174:3650.
32 Makeyev, A. V. and Liebhaber, S. A. 2002. The poly(C)-binding proteins: a multiplicity of functions and a search for mechanisms. *RNA* 8:265.
33 Makeyev, A. V., Chkheidze, A. N. and Liebhaber, S. A. 1999. A set of highly conserved RNA-binding proteins, alphaCP-1 and alphaCP-2, implicated in mRNA stabilization, are coexpressed from an intronless gene and its intron-containing paralog. *J. Biol. Chem.* 274:24849.
34 Mahtani, K. R., Brook, M., Dean, J. L., Sully, G., Saklatvala, J. and Clark, A. R. 2001. Mitogen-activated protein kinase p38 controls the expression and posttranslational modification of tristetraprolin, a regulator of tumor necrosis factor alpha mRNA stability. *Mol. Cell. Biol.* 21:6461.
35 Collier, B., Goobar-Larsson, L., Sokolowski, M. and Schwartz, S. 1998. Translational inhibition *in vitro* of human papillomavirus type 16 L2 mRNA mediated through interaction with heterogenous ribonucleoprotein K and poly(rC)-binding proteins 1 and 2. *J. Biol. Chem.* 273:22648.
36 Perrotti, D., Cesi, V., Trotta, R. *et al.* 2002. BCR-ABL suppresses C/EBPalpha expression through inhibitory action of hnRNP E2. *Nat. Genet.* 30:48.
37 Ostareck, D. H., Ostareck-Lederer, A., Wilm, M., Thiele, B. J., Mann, M. and Hentze, M. W. 1997. mRNA silencing in erythroid differentiation: hnRNP K and hnRNP E1 regulate 15-lipoxygenase translation from the 3' end. *Cell* 89:597.

THE JOURNAL OF COMPARATIVE NEUROLOGY 502:275–290 (2007)

Clustering, Migration, and Neurite Formation of Neural Precursor Cells in the Adult Rat Hippocampus

TATSUNORI SEKI,[1]* TAKASHI NAMBA,[1,2] HIDEKI MOCHIZUKI,[3,4] AND MASAFUMI ONODERA[5]

[1]Department of Anatomy, Juntendo University School of Medicine, Tokyo, Japan
[2]Major in Integrative Bioscience and Biomedical Engineering, School of Science and Engineering, Waseda University, Tokyo, Japan
[3]Department of Neurology, Juntendo University School of Medicine, Tokyo, Japan
[4]Research Institute for Diseases of Old Ages, Juntendo University School of Medicine, Tokyo, Japan
[5]Department of Hematology, Institute of Clinical Medicine, University of Tsukuba, Ibaraki, Japan

ABSTRACT

Adult neurogenesis occurs in the subgranular zone and innermost part of the dentate granule cell layer. To examine how neural precursor cells proliferate, migrate, and extend their neurites, we performed BrdU- and improved retrovirus-green fluorescence protein (GFP)-labeling analyses. Soon after labeling the majority of BrdU+ cells and GFP+ cells expressed Ki67, a cell cycle marker, and formed clusters together with PSA+ neuroblasts. Most of the Ki67+ proliferating cells expressed Hu, an immature and mature neuronal marker, and the subpopulation expressed both Hu+ and GFAP+. In the clusters, Ki67+ and PSA+ cells strongly expressed β-catenin and N-cadherin, but PSA+ cells outside the clusters did not. Therefore, it was mainly Hu+ neuronal precursor cells that proliferated within clusters in which the cluster cells are closely associated via cell adhesion molecules, such as N-cadherin/β-cateninIn and PSA. The newly generated cells appeared to stay in the clusters for a few days and then disperse around the clusters. The findings of this in vivo analysis and in vitro time-lapse imaging of early postnatal hippocampal slices support the notion that most postmitotic neuroblasts migrate tangentially from clusters, extending tangentially oriented processes, one of which often retains close contact with the clusters, and finally extend radial processes, or prospective apical dendrites. These results suggest that the clustering cells and tangentially migrating cells have a systematic cellular arrangement and intercellular interaction. J. Comp. Neurol. 502:275–290, 2007. © 2007 Wiley-Liss, Inc.

Indexing terms: adult neurogenesis; clustering; migration; PSA; catenin; Hu; retrovirus; EGFP; tangential migration

Neurogenesis continues along the border between the granule cell layer (GCL) and hilus of the adult dentate gyrus (Altman and Das, 1965; Kaplan and Hinds, 1977; Seki and Arai, 1991b, 1993, 1995; Cameron et al., 1993; Kuhn et al., 1996; Gould and Gross, 2002). Recently, extensive studies have revealed that the neural progenitors in the adult hippocampus have astrocytic features (Seri et al., 2001; Filippov et al., 2003; Fukuda et al., 2003; Garcia et al., 2004) and develop into mature neurons through a series of steps (Seki, 2002b; van Praag et al., 2002; Fukuda et al., 2003; Kempermann et al., 2004a; Alvarez-Buylla and Lim, 2004; Esposito et al., 2005; Shapiro and Ribak, 2005; Tozuka et al., 2005; Zhao et al., 2006). Additionally, it has been proposed that there are adult neurogenic niches that maintain neurogenesis throughout life (Palmer et al., 2000; Song et al., 2002; Mercier et al., 2002;

Grant sponsor: Japan Society for the Promotion of Science Grant-in-Aid for Scientific Research; Grant number: 17500238; Grant sponsor: High Technology Research Center Grant from the Japanese Ministry of Education, Culture, Sports and Science.

*Correspondence to: Tatsunori Seki, Department of Anatomy, Juntendo University School of Medicine, 2-1-1 Hongo, Bunkyo, Tokyo 113-8421, Japan. E-mail: tseki@med.juntendo.ac.jp

Received 14 March 2006; Revised 15 September 2006; Accepted 15 December 2006

DOI 10.1002/cne.21301

Published online in Wiley InterScience (www.interscience.wiley.com).

© 2007 WILEY-LISS, INC.

Doetsch, 2003; Seki, 2003; Shen et al., 2004; Alvarez-Buylla and Lim, 2004). It is also known that adult neurogenesis is regulated by various factors, such as the external environment, hormones, and brain injury (Parent, 2003; Kempermann et al., 2004b; Abrous et al., 2005; Doetsch and Hen, 2005; Shapiro and Ribak, 2005).

However, the exact cellular arrangement and intercellular relationship of neurogenesis, as has been clearly shown in the developing neocortex (Rakic, 1971, 2003; Marin-Padilla, 1998; Miyata et al., 2001; Tamamaki et al., 2001; Fujita, 2003; Tabata and Nakajima, 2003; Noctor et al., 2004), still remains to be explored in the adult hippocampus. In particular, it is not yet precisely known how the neural precursors proliferate and then migrate from the site of cell proliferation to develop neurites. In this respect, we have previously found that proliferating cells are buried in the tangential processes of polysialic acid-positive (PSA+) neuroblasts and immature neurons in 2-month-old rats (Seki, 2002b). However, we could not describe the exact developmental sequence from proliferating cells to immature neurons because in relatively young adult rats the dentate subgranular zone (SGZ) contains many proliferating cells and neuroblasts, forming a dense plexus of tangential processes.

To overcome this problem, in the present BrdU experiments we used older rats at the age of 6 months since the number of PSA-expressing neuroblasts and immature neurons is decreased at that age (Seki and Arai, 1995; Kuhn et al., 1996; Seki, 2002a). This allows the relation between proliferating cells and postmitotic neuroblasts migrating from the proliferative sites to be readily recognized. In another type of experiment, we used retrovirus-green fluorescence protein (GFP), which labels a subset of proliferating cells and reveals morphological details of the newly generated cells (Tanaka et al., 2004; Esposito et al., 2005; Namba et al., 2005; Zhao et al., 2006). Additionally, to observe migration and neurite formation directly, time-lapse imaging of GFP-labeled cells was performed in a slice culture of the early postnatal hippocampus. The results of the present study support the notion that neuronal precursors mainly proliferate within cell clusters, then move mainly tangentially from the cell proliferation site, leaving a trailing process behind at the proliferation site, after which they finally extend radially oriented dendrites.

MATERIALS AND METHODS

Animals

Male Wistar rats at 2 and 6 months of age were purchased from Japan SLC and maintained in the animal care centers of Juntendo University. All animal treatments were approved by the Institutional Animal Care and Use Committee at our institution.

BrdU injection

The rats were given an intraperitoneal (i.p.) injection of BrdU (Sigma, St. Louis, MO) dissolved in 0.9% NaCl (50 mg/Kg body weight). One, 3, 6, and 7 days after the BrdU injections the rats were deeply anesthetized with sodium pentobarbital and perfused intracardially: first with 0.01 M phosphate-buffered saline (PBS), pH 7.4, followed by 4% paraformaldehyde in 0.1 M phosphate buffer (PB), pH 7.4, at room temperature.

Retrovirus injection

An improved retroviral vector was prepared using 293 gpg/ENEGFP, a 293 gpg cell line transduced with DNEGFP, which is an expression vector carrying enhanced green fluorescent protein (EGFP), by a previously described method (Suzuki et al., 2002; Tanaka et al., 2004). Rats at the age of 8 weeks were anesthetized with pentobarbital. Improved retrovirus carrying EGFP (0.5 μL at the rate of 0.1 μL/min) was stereotaxically injected into both sides of the dentate gyrus (posterior, 3.5–4.0 mm from bregma; lateral, 2.0–2.5 mm; ventral, 3.5–4.0 mm). Two, 3, 4, and 5 days after the retrovirus injection the rats were fixed as described above.

Tissue preparations

Brains were removed from the skull and postfixed overnight in the same solution at 4°C. The fixed brains were washed with PBS and the cerebral cortices containing the hippocampal formation were dissected away from the remaining brain structure. Next, 1–2-mm-thick slices were cut in a plane perpendicular to the septotemporal axis of the hippocampal formation at the approximate midpoint of the axis. For storage, the thick slices were immersed in 10% sucrose for 2–5 hours, then in 20% sucrose in PBS at 4°C overnight, embedded in OCT compound, and stored at −70°C. Before sectioning the samples were thawed, washed in PBS, and embedded in 5% agarose in PBS. The hippocampus was cut by a vibratome into 50-μm sections. The vibratome sections were stored in a solution of 30% ethylene glycol, 25% glycerin in 0.1 M PB at −40°C.

Antibodies

The species, class, dilution, and vendor (catalog number) of antibodies used are shown in Table 1. The monoclonal anti-BrdU was generated in rats. This antibody reacts with BrdU in single-stranded DNA, BrdU attached to a protein carrier, or free BrdU, but does not crossreact with thymidine (manufacturer's technical information). No staining was seen in the brain of rats not injected with BrdU. The rabbit polyclonal anti-β-catenin was developed using a synthetic peptide (Pro-Gly-Asp-Ser-Asn-Gln-Leu-Ala-Trp-Phe-Asp-Thr-Asp-Leu) conjugated to KLH as immunogen. The peptide corresponds to amino acids 768–781 of human or mouse β-catenin. The antibody reacts with a 94-kD protein using immunoblotting and shows no crossreactivity with α-catenin peptide (amino acids 890–901) conjugated to bovine serum albumin (BSA). Specific staining in immunoblotting is inhibited following preincubation of the diluted antiserum with the β-catenin peptide (manufacturer's technical information). The β-catenin immunoreactivity in the hippocampus was very similar to that reported previously (Madsen et al., 2003). The mouse monoclonal anti-GFAP was generated against purified GFAP from pig spinal cord. This antibody specifically localizes GFAP in an immunoblot technique and does not crossreact with vimentin. The antibody stains astrocytes, Bergmann glia cells, and gliomas (manufacturer's technical information). The rabbit polyclonal anti-GFAP was generated against GFAP isolated from cow spinal cord. The antibody is specific to astrocytes (i.e., glial cells) and ependymal cells of the central nervous system (manufacturer's technical information). These two antibodies to GFAP only stained cells with the classic morphology and

TABLE 1. Antibodies*

Antibodies	Species/class	Dilution	Vendor (catalog No) or references
Primary antibodies			
BrdU	Rat IgG	1:400	ImmunologicalsDirect.com (OBT0030)
β-catenin	Rabbit IgG	1:2000	Sigma (C2206)
GFAP	Mouse IgG	1:2000	Sigma (G3893)
GFAP	Rabbit IgG	1:200	NeoMarkers (RB-087-A0)
GFP	Rabbit IgG	1:100	Tamamaki et al. 2000
GFP	Rabbit IgG	1:400	Chemicon (AB3080)
Hu	Human IgG	1:2000	Okano et al. 1997
Ki67	Mouse IgG	1:200	Novocastra Laboratories (NCL-Ki67-MM1)
Ki67	Rabbit IgG	1:200	Novocastra Laboratories (NCL-Ki67p)
MASH-1	Mouse IgG	1:200	BD Bioscience (556604)
N-cadherin	Mouse IgG	1:1000	BD Bioscience (610920)
PSA	Mouse IgM	1:500	Seki and Arai, 1991
S100-β	Mouse IgG	1:2000	Sigma (S2532)
Secondary antibodies			
Human IgG (H+L) + Cy3	donkey	1:200	Jackson (709-165-149)
Human IgG (H+L) + Cy5	donkey	1:200	Jackson (709-175-149)
Mouse IgG (H+L) + Cy2	donkey	1:200	Jackson (715-225-151)
Mouse IgG (H+L) + Cy3	donkey	1:200	Jackson (715-165-151)
Mouse IgG (H+L) + Cy5	donkey	1:200	Jackson (715-175-151)
Mouse IgG (γ) +Cy3	goat	1:200	Jackson (115-165-071)
Mouse IgM (μ) +Cy2	goat	1:200	Jackson (115-225-075)
Mouse IgM (μ) +Cy5	goat	1:200	Jackson (715-175-140)
Rabbit IgG (H+L) + FITC	donkey	1:200	Jackson (711-095-152)
Rabbit IgG (H+L) + Cy3	donkey	1:200	Jackson (711-165-152)
Rat IgG (H+L) + Cy3	donkey	1:200	Jackson (712-165-153)

*The immunization antigens and specificity of the antibodies are described in Materials and Methods.

distribution of fibrillary astrocytes (Kosaka and Hama, 1986) and cells with radial processes (radial glia-like cells) in the hippocampus (Schmidt-Kastner and Szymas, 1990). The rabbit polyclonal anti-GFP (Tamamaki et al., 2000) was generated against GFP that was induced in *E. coli* with full-length GFP coding sequence and purified according to the protocol recommended by the manufacturer of the GST-system (Amersham-Pharmacia Biotech, Piscataway, NJ). The rabbit monoclonal anti-GFP (Chemicon, Temecula, CA) was generated against GFP conjugated to BSA. The antibody reacts with various forms of GFP including EGFP including those found in vectors supplied by ClonTech (Palo Alto, CA) and Invitrogen (Carlsbad, CA; manufacturer's technical information). The two antibodies to GFP did not stain the brain of rats not injected with retrovirus-GFP. The human anti-Hu was obtained from patient serum of paraneoplastic neurological syndrome (the Hu syndrome) and was purified using the full-length HuC fusion protein coupled covalently to cyanogen bromide Sepharose 4B (Pharmacia, Uppsala, Sweden) according to the manufacturer's instructions (Okano and Darnell, 1997). The Hu antiserum detects recombinant fusion proteins of all four Hu family members and also recognizes a set of antigens of 35–40 kD on Western blots of brain. Immunofluorescence double exposure of GFAP and Hu immunoreactivity in the adult neocortex has demonstrated that the two are mutually exclusive (Okano and Darnell, 1997). The mouse monoclonal anti-Ki67 and the rabbit polyclonal anti-Ki67 were generated using prokaryotic recombinant fusion protein corresponding to a 1,086-bp Ki67 motif-containing cDNA (manufacturer's technical information). A double band at 245–395 kD is detected by Western blot analysis (Key et al., 1993). Two hours after BrdU injection all BrdU-labeled cells were stained with these antibodies and the number of the double-positive cells was reduced 7 days after the BrdU injection. The mouse monoclonal anti-MASH-1, a product of proneuronal gene, recognizes mouse and rat MASH1. Recombinant, full-length rat MASH1 protein was used as immunogen. The antibody identifies a 34-kD band in Western blot analysis of lysate from rat embryonic brain (manufacturer's technical information). The staining with the anti-MASH1 was confined to nuclei of neurogenic regions in the adult hippocampus. The distribution pattern of MASH1-immunoreactive cells in the adult hippocampus was very similar to that of MASH1 mRNA (Pleasure et al., 2000). The mouse monoclonal anti-N-cadherin was generated from amino acids 802–819 of mouse N-cadherin and recognizes a band of 130 kD protein in Western blot analysis of rat brain (manufacturer's technical information). The distribution of cells stained with this antibody in the dentate gyrus was very similar to that detected with other antibodies to N-cadherin (Shan et al., 2002). The staining with this antibody was colocalized with that of β-catenin that binds to cytoplasmic domain of N-cadherin. The mouse monoclonal anti-PSA was generated against a living cell suspension from the forebrain of an embryonic day 18 Wistar rat (Seki and Arai, 1991a). The antibody recognizes a 180–280-kD broad band because of the negative charge of polysialic acid. The characterization of the antigenic specificity of this antibody using lipid-conjugated oligo/polysialic acids has shown that the minimum chain length required for antigen-antibody binding is 5 N-actylneuraminic acid residues (Sato et al., 1995). Endo N, PSA-specific endoneuraminidase abolishes the immunostaining by this antibody in the hippocampus (Seki and Rutishauser, 1998). The mouse monoclonal anti-S100β was generated using purified bovine brain S-100β preparation. This antibody recognizes an epitope located on the β-chain, but not on the α-chain of S-100 and does not react with other members of the EF-hand family such as calmodulin, parvalbumin, intestinal calcium-binding protein, and myosin light chain (manufacturer's technical information). The antibodies to S100β stained cells with the classic morphology and distribution of astrocytes and cells with radial processes (radial glia-like cells) in the hippocampus, as reported previously (Schmidt-Kastner and Szymas, 1990).